

# The importance of the adiabatic index in modeling strains and stresses in spinning-down pulsars

E. Giliberti<sup>1,4\*</sup>, G. Cambiotti<sup>2</sup>, M. Antonelli<sup>3</sup> † and P.M. Pizzochero<sup>1,4</sup>

<sup>1</sup>*Dipartimento di Fisica, Università degli Studi di Milano, Via Celoria 16, 20133, Milano, Italy*

<sup>2</sup>*Dipartimento di Scienze della Terra, Università degli Studi di Milano, Via Cicognara 7, Milano, 20129, Italy*

<sup>3</sup>*Nicolaus Copernicus Astronomical Center, ul. Bartycka 18, 00-716 Warsaw, Poland*

<sup>4</sup>*Istituto Nazionale di Fisica Nucleare, sezione di Milano, Via Celoria 16, 20133 Milano, Italy*

14 March 2019

## ABSTRACT

We introduce a Newtonian model for the deformations of a compressible and stratified neutron star that goes beyond the widely used Cowling approximation. We employ this model to study the role played by the adiabatic index in the calculation of rotation-induced deformations: we assume a polytropic equation of state for the matter at chemical equilibrium but, since the equilibrium reactions may be slow, the perturbations with respect to the unstressed configuration are modeled by using an equation of state with a different polytropic index. Hence, we quantify the impact of a departure of the adiabatic index from its equilibrium value on the calculated stresses and strains. We obtain that a small variation in the adiabatic index which regulates the perturbation can cause large variations in the calculated displacements and strains, the effect being larger for lighter stars. As a first practical application of our model, we estimate the strain developed between consecutive glitches in the Vela pulsar, confirming the known difficulty that arises when trying to explain the trigger of pulsar glitches with starquakes: in order for the quake to be a possible trigger, the solid crust must never fully relax after a glitch, making the sequence of starquakes in a neutron star an history-dependent process.

**Key words:** stars: neutron - pulsars: general

## 1 INTRODUCTION

Neutron stars (NSs) possess a solid crust which has elastic properties and may be stressed under the action of external loads, like the centrifugal force due to rotation, the presence of mountains or intense and localized magnetic fields (for a comprehensive review of the neutron star crusts properties see e.g. [Chamel & Haensel 2008](#)).

The sudden setting of this crust in a strong gravitational field is a key aspect for the modeling of many astronomical phenomena related to neutron stars, such as glitches ([Ruderman 1976](#)) and flares ([Blaes et al. 1989](#)), the possible neutron star precession ([Pines 1974](#); [Cutler et al. 2003](#)) and the emission of gravitational waves ([Lasky 2015](#); [Fatoyev et al. 2018](#)), which may have direct consequences on the observed braking indexes of pulsars ([Woan et al. 2018](#)). Stresses slowly build-up in the crust till a certain threshold, defined by the so-called *breaking strain* ([Christensen 2013](#)), is reached. At this point the elastic behaviour of the lattice

abruptly ceases because of fault formations and a portion of the crust settles down under gravity to a less-stressed configuration. This process is known as *starquake* and it is sometimes invoked as the cause of small glitches or the trigger of glitches in pulsars and of bursts in magnetars (see e.g. [Baym et al. 1969](#); [Ruderman 1991b](#); [Thompson & Duncan 1995](#); [Lander et al. 2015](#); [Keer & Jones 2015](#)). This starquake hypothesis is supported by different studies, underlining that glitch sizes ([Melatos et al. 2008](#); [Howitt et al. 2018](#)) and burst-energy distribution follow a power law ([Cheng et al. 1996](#); [Göğüş et al. 2000](#)), as do earthquakes on Earth. The quakes may also drive NS’s precession, as explored in the work of [Ushomirsky et al. \(2000\)](#), as well as the evolution of the magnetic field (see e.g. [Link et al. 1998](#); [Lander & Gourgoullos 2019](#)). On the other hand, the rigid crust can sustain tri-axial deformations (referred to as *mountains* in the literature, see e.g. [Haskell et al. 2006](#)), which size may be enough to emit detectable gravitational waves in the near future ([Abbott et al. 2017](#)).

Despite such a large use of the crust failure hypothesis, there is still a lack of “realistic” and quantitative models for the study of crust deformations under different types of load-

\* [elia.giliberti@unimi.it](mailto:elia.giliberti@unimi.it)

† [mantonelli@camk.edu.pl](mailto:mantonelli@camk.edu.pl)

ing forces. The nature of those loads can vary, ranging from the non-uniform centrifugal force to the stresses induced by the magnetic field evolution and possibly by pinning of superfluid vortices to the crustal lattice (see e.g. the seminal work of Ruderman 1991a).

To date, most of the studies rely on different approximations, either in the neutron star structure description, where the star is idealized as a uniform elastic sphere (see e.g. Gilbert & Backus 1968; Franco et al. 2000; Fattoyev et al. 2018), a two-layers sphere (Giliberti et al. 2018) or for using the Cowling approximation (as in Ushomirsky et al. 2000). As a first step towards a better and more consistent description of these issues, we present a Newtonian model for the calculation of NS's crust deformation. This model has been already successfully used for the Earth (Sabadini et al. 2016) and it is here adapted and applied to neutron stars.

In order to account for stratification and different elastic properties of matter, our model allows for an arbitrarily large number of layers with different values of the bulk and shear modulus, varying with continuity inside every layer. Clearly, the equilibrium stratification of matter can be calculated by solving the hydrostatic equilibrium equations, once an equation of state is provided (Shapiro & Teukolsky 1983). For a given equation of state, it is possible to define a related adiabatic index: this fundamental quantity appears into the equations governing small-amplitude NSs pulsations (Thorne & Campolattaro 1967) and in a relativistic context it provides a criteria of stability for cold stars (Meltzer & Thorne 1966; Chanmugam 1977; Gourgoulhon et al. 1995). When the star is perturbed around the hydrostatic equilibrium configuration, it is known that the appropriate  $\gamma$  must be calculated by taking into account the possible slowness of the equilibration channels, typically mediated by the weak interaction (Haensel et al. 2007): for the time-dependent perturbations (i.e. NSs oscillations),  $\gamma$  is not simply the one defined by the equation of state at equilibrium as any change in density disturbs beta equilibrium; in particular, it has been proposed that this departure of  $\gamma$  from its equilibrium value provides an effective viscous damping of NS oscillations (Haensel et al. 2002). Therefore, we apply our model to discuss how a departure of the adiabatic index  $\gamma$  for its equilibrium value may affect the estimate of the stresses in a spinning-down pulsar.

The paper is organized as follows: in sections 2 and 3 we introduce the main equations of the model, discussing how a departure of the adiabatic index from the value at chemical equilibrium, in the sense provided by Haensel et al. (2002), can be expected during the gradual development of stresses. In section 4 we discuss the boundary conditions of the model and write the general elastic solution of the problem. Section 5 is devoted to the calculation of displacements and strains *due to an uniform rotation*, for the polytropic equation of state (EoSs) with  $n = 1$ . Finally, in section 6 we focus on the strain developed by an isolated NS between two glitches, similarly to what has been done by means of a simpler analytical model in Giliberti et al. (2018).

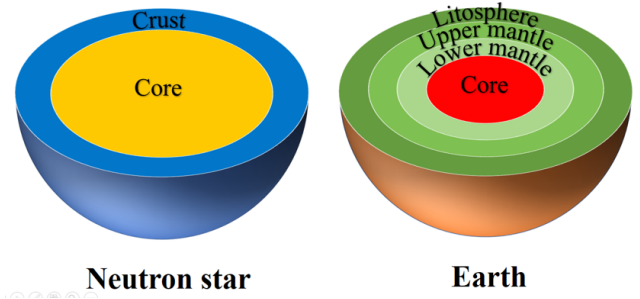


**Figure 1.** We model a NS as an object with only two layers: a fluid core and an elastic crust. However, the proposed equations allow to introduce an arbitrary large number  $n$  of elastic layers, as shown in the schematic representation of the Earth: better comprehension of the elastic properties of a NS crust will allow to introduce additional layers, e.g. the shell containing the pasta phase at the bottom of the crust. In principle our model allows to treat continuous stratification of both density and elastic coefficients.

## 2 MAIN EQUATIONS

Our aim is to describe the deformations of a compressible and self-gravitating neutron star under the effect of specified forces in a Newtonian framework. We assume to have an object with an internal core that is fluid, topped by a number of stratified layers with different elastic properties. For example, as sketched in Fig 1, for the Earth we have a lithosphere, an upper mantle and a lower mantle. For our purposes, in this work we describe the model in its full generality (which may be useful for future more refined studies) but in the numerical calculations we model a NS with a single elastic layer, the crust.

The generality of this approach allows to consider tidal and centrifugal forces and other non-conservative forces (like vortex pinning to impurities in the crust). Moreover, it is possible to introduce also loads which account for inhomogeneities inside the star (the so-called *bulk* loads), as well as *surface* loads (which are useful to model the compressional effect of mountains on the Earth). In the framework of NS physics, these particular loads can be used to study the effect of accretion of matter onto the crust, making the inclusion of these forces potentially interesting. Unfortunately, it is known that these kind of loads need a specific technique to handle the boundary conditions (Sabadini et al. 2016), so that we will not include them here in order to maintain the discussion self-contained.

We start by considering the momentum and Poisson equations for our system, comprised by a NS and (possibly) an additional companion, namely

$$\nabla \cdot \boldsymbol{\tau} - \rho \nabla \Phi + \mathbf{h} = 0 \quad (1)$$

$$\nabla^2 \Phi = 4\pi G (\rho + \rho^T) + 2\Omega^2 \quad (2)$$

where  $\boldsymbol{\tau}$  is the Cauchy stress tensor describing surface forces,  $\mathbf{h}$  are the non-conservative body forces, and  $\rho$ ,  $\rho^T$  are the density of the NS and of the companion respectively. The potential  $\Phi$  encodes all the conservative body forces and can be split as

$$\Phi = \phi + \phi^C + \phi^T \quad (3)$$

with  $\phi$  being the gravitational potential due to the density distribution of the NS,  $\phi^T$  the one due to the companion (also called *tidal* potential) and  $\phi^C$ , the centrifugal potential. In particular we have that  $\nabla^2 \phi^C = 2\Omega^2$ , where  $\Omega$  is the angular velocity of the NS.

In the absence of a companion, we take as reference configuration the one defined by the hydrostatic equilibrium of the NS and we introduce a displacement field  $\mathbf{u}$  which describes perturbations with respect to the reference position  $\mathbf{x}$ , namely

$$\mathbf{r} = \mathbf{x} + \mathbf{u}(\mathbf{x}), \quad (4)$$

where  $\mathbf{x}$  and  $\mathbf{r}$  are the initial and the perturbed positions of the infinitesimal matter elements. Hence, the total stress tensor can be expressed as<sup>1</sup>

$$\boldsymbol{\tau}(\mathbf{r}) = -P_0(\mathbf{x}) \mathbf{1} + \boldsymbol{\tau}^\delta(\mathbf{x}), \quad (5)$$

where  $P_0$  is the initial hydrostatic pressure (cf. Zdunik et al. 2008). We indicate with  $\mathbf{1}$  the identity tensor and with  $\boldsymbol{\tau}^\delta$  the material stress given by Hooke's law (Love 1934; Landau & Lifshitz 1970; Sabadini et al. 2016)

$$\boldsymbol{\tau}^\delta = (\kappa - 2/3\mu)(\nabla \cdot \mathbf{u})\mathbf{1} + \mu(\nabla \mathbf{u} + (\nabla \mathbf{u})^T), \quad (6)$$

$\kappa$  and  $\mu$  being the bulk and shear moduli respectively. The transpose operation is indicated by the symbol  $T$ .

For a given initial density  $\rho_0$ , hydrostatic pressure  $P_0$  and gravitational potential  $\phi_0$  of the unstressed NS, the momentum (1) and Poisson (2) equations are

$$\nabla P_0 + \rho_0 \nabla \phi_0 = 0 \quad (7)$$

$$\nabla^2 \phi_0 = 4\pi G \rho_0. \quad (8)$$

This system defines the initial state of hydrostatic equilibrium for a non-rotating star: the functions  $P_0$ ,  $\rho_0$  and  $\phi_0$  are spherically symmetric.

Following the notation used in Sabadini et al. (2016), let us introduce the local incremental density  $\rho^\Delta$  and the total potential  $\Phi^\Delta$  of the NS

$$\rho(\mathbf{r}) = \rho_0(\mathbf{r}) + \rho^\Delta(\mathbf{r}) \quad (9)$$

$$\Phi(\mathbf{r}) = \Phi_0(\mathbf{r}) + \Phi^\Delta(\mathbf{r}) \quad (10)$$

The first is related to the displacement  $\mathbf{u}$  via mass conservation

$$\rho^\Delta = -\nabla \cdot (\rho_0 \mathbf{u}), \quad (11)$$

while the other is the local *incremental* potential

$$\Phi^\Delta = \phi^\Delta + \phi^C + \phi^T, \quad (12)$$

which, in addition to the incremental gravitational potential of the NS, includes also the centrifugal  $\phi^C$  and tidal  $\phi^T$  contributions. After substitution of Eqs (7) and (8) into Eqs

(1) and (2) and making use of (11) we obtain the incremental momentum and Poisson equations

$$\nabla \cdot \boldsymbol{\tau}^\delta - \nabla \cdot (\rho_0 \mathbf{u} \cdot \nabla \phi_0) + \nabla \cdot (\rho_0 \mathbf{u}) \nabla \phi_0 - \rho_0 \nabla \Phi^\Delta + \mathbf{h} = 0 \quad (13)$$

$$\nabla^2 \Phi^\Delta = 4\pi G(-\nabla \cdot (\rho_0 \mathbf{u}) + \rho^T) + 2\Omega^2. \quad (14)$$

In order to obtain the above equations we used the definitions provided in Eqs (6), (9), (10) and we performed a linear expansion in the displacement field (i.e. all the non-linear terms in the perturbed quantities have been neglected).

In our case of a nearly spherical body, the symmetry of the problem simplifies the treatment of the above equations: we introduce the usual spherical coordinate system  $\{r, \theta, \varphi\}$ , that are the radial distance from the center of the NS, the co-latitude and the longitude of a point respectively. Hence, we expand the potential  $\Phi^\Delta$  and the displacement  $\mathbf{u}$  in spherical harmonics (see Appendix A for the conventions used). We underline that in the initial hydrostatic equilibrium the elastic parameters  $\kappa$  and  $\mu$  are functions of the coordinate  $r$  only. Thanks to the expansion in spherical harmonics  $Y_{\ell m}$  and some amount of algebra, Eq (13) can be rearranged as

$$\begin{aligned} & -\rho_0 \partial_r \Phi_{\ell m} - \rho_0 \partial_r (g U_{\ell m}) + \rho_0 g \chi_{\ell m} + \\ & \partial_r \left[ \left( \kappa - \frac{2}{3}\mu \right) \chi_{\ell m} + 2\mu \partial_r U_{\ell m} \right] + \\ & \frac{1}{r^2} \mu [4r \partial_r U_{\ell m} - 4U_{\ell m} + \ell(\ell+1)(3V_{\ell m} - U_{\ell m} - r \partial_r V_{\ell m})] + \\ & h_{\ell m}^R = 0 \end{aligned} \quad (15)$$

$$\begin{aligned} & -\frac{\rho_0}{r} \Phi_{\ell m} - \frac{\rho_0}{r} g U_{\ell m} + \frac{(\kappa - \frac{2}{3}\mu)}{r} \chi_{\ell m} + \\ & \partial_r \left[ \mu \left( \partial_r V_{\ell m} + \frac{1}{r} U_{\ell m} - \frac{1}{r} V_{\ell m} \right) \right] + \\ & \frac{1}{r^2} \mu [5U_{\ell m} + 3r \partial_r V_{\ell m} - V_{\ell m} - 2\ell(\ell+1)V_{\ell m}] + \\ & h_{\ell m}^S = 0, \end{aligned} \quad (16)$$

$$\begin{aligned} & \partial_r \left[ \mu \partial_r W_{\ell m} - \frac{\mu W_{\ell m}}{r} \right] + \frac{3\mu}{r} \partial_r W_{\ell m} - \\ & \frac{1+\ell(\ell+1)}{r^2} \mu W_{\ell m} + h_{\ell m}^T = 0. \end{aligned} \quad (17)$$

In the above equations  $U_{\ell m}$ ,  $V_{\ell m}$  and  $W_{\ell m}$  are the radial, tangential and toroidal displacements,  $h_{\ell m}^R$ ,  $h_{\ell m}^S$ ,  $h_{\ell m}^T$  are the spherical expansion components of the non-conservative forces and the scalars  $\chi_{\ell m}$  are linked to the volume change  $\Delta$  according to

$$\Delta = \nabla \cdot \mathbf{u} = \sum_{\ell=0}^{\infty} \sum_{m=-\ell}^{\ell} \chi_{\ell m} Y_{\ell m}. \quad (18)$$

The radial (15) and tangential (16) components of the equilibrium equations are called *spheroidal equations* while the third component (17) is called *toroidal equation*. With a similar treatment the Poisson equation (14) becomes

$$\nabla_r^2 \Phi_{\ell m} = -4\pi G(\rho_0 \chi_{\ell m} + U_{\ell m} \partial_r \rho_0) + 4\pi G \rho_{\ell m}^T, \quad (19)$$

<sup>1</sup> In this work and in Giliberti et al. (2018) we adopt the notation described in Sabadini et al. (2016): for a generic quantity  $f$ , the “local increment”  $f^\Delta$  coincides with what is usually called Eulerian change (see e.g. Shapiro & Teukolsky 1983). On the other hand, the Lagrangian changes of  $f$  are dubbed “material increments” and are indicated by  $f^\delta$ .

where

$$\nabla_r^2 = \partial_r + \frac{2}{r}\partial_r - \frac{\ell(\ell+1)}{r^2} \quad (20)$$

and  $\rho_{\ell m}^T$  are the density spherical harmonics coefficients of the NS companion. The Eqs (15, 16, 17, 19) hold only for  $\ell > 0$ ; the case  $\ell = 0$  needs a specific treatment, as shown in detail in Appendix B. Furthermore, we underline that the toroidal equation (17) is decoupled from Eqs (15, 16, 19). Since in this initial work we are interested only on the effect of rotation, this fact allows us to neglect the toroidal equation. In fact only some kind of non-conservative forces, having non-axial symmetry, can have an impact on the toroidal equation (Sabadini et al. 2016). It is very useful to recast the remaining three equations (15, 16, 19), that are second order in  $U_{\ell m}, V_{\ell m}, \Phi_{\ell m}$ , into six differential equations of the first order. Having this in mind, we introduce the spheroidal 6-vector solution  $\mathbf{y}_{\ell m}$

$$\mathbf{y}_{\ell m} = (U_{\ell m}, V_{\ell m}, R_{\ell m}, S_{\ell m}, \Phi_{\ell m}, Q_{\ell m})^T. \quad (21)$$

As shown in Appendix A, the meaning of the six components is as follows: the first and the second components are the radial and tangential displacements, the third and the fourth the radial and tangential stresses, the fifth is the potential while the sixth, dubbed *potential stress*  $Q_{\ell m}$ , is defined by

$$Q_{\ell m} = \partial_r \Phi_{\ell m} + \frac{\ell+1}{r} \Phi_{\ell m} + 4\pi G \rho_0 U_{\ell m}. \quad (22)$$

The term  $(\ell+1)\Phi_{\ell m}/r$  has been included for simplifying the boundary conditions, as discussed in section 4. Thanks to the definition (21), the whole system of equations (15, 16, 19) can be written in the more compact form

$$\frac{d\mathbf{y}_{\ell m}}{dr} = \mathbf{A}_{\ell}(r) \mathbf{y}_{\ell m}(r) - \mathbf{h}_{\ell m}(r). \quad (23)$$

Here  $\mathbf{A}_{\ell}$  is a  $6 \times 6$  matrix containing the elastic characteristic quantities (the bulk modulus and the shear modulus), the initial configuration profiles for the density and the gravitational acceleration field (see Appendix C). The non-homogeneous term  $\mathbf{h}_{\ell m}$  in equation (23) is

$$\mathbf{h}_{\ell m} = (0, 0, h_{\ell m}^R, h_{\ell m}^S, 0, 0)^T. \quad (24)$$

In order to maintain the description general and potentially useful to describe also non-symmetric problems, we explicit the index  $m$  in the following, despite the fact that the centrifugal force has axial symmetry<sup>2</sup> (i.e. in its expansion the only non-zero coefficients are the ones with  $m = 0$ ).

### 3 MODELING THE RESPONSE OF MATTER

Following the standard description for cold catalyzed matter in a NS interior, we consider here a barotropic EoS of the kind  $P(n_b), \rho(n_b)$ , where  $n_b$  is the local baryon density. In particular, the pressure can be obtained as

$$P(n_b) = n_b^2 \frac{d}{dn_b} \frac{E(n_b)}{n_b}, \quad (25)$$

<sup>2</sup> This general statement of the model, in fact, is very useful when loads don't have any particular symmetry, like dislocations induced by starquakes.

where  $E(n_b)$  the ground state energy density at fixed equilibrium composition. The equation of state for matter at chemical equilibrium is characterized by the adiabatic index  $\gamma_{eq}$ , defined as

$$\gamma_{eq}(n_b) = \frac{n_b}{P} \frac{\partial P(n_b)}{\partial n_b}. \quad (26)$$

Hence,  $\gamma_{eq}$  can be used to describe pressure-density perturbations which dynamics is very slow with respect to the typical timescales of the interactions<sup>3</sup> that carry the system towards the full thermodynamic equilibrium.

The opposite limit, in which all the chemical reactions are so slow that can be considered frozen, is also interesting for astrophysical studies. However, in this case the relation Eq (26) cannot be used to define the proper adiabatic index which regulates the pressure-density perturbations. The corresponding adiabatic index  $\gamma_f$ , where the subscript  $f$  stands for *frozen*, now depends also on the chemical fractions  $x_i$  for the  $i$ -species:

$$\gamma_f(n_b, x_i) = \frac{n_b}{P} \frac{\partial P(n_b, x_i)}{\partial n_b}, \quad (27)$$

where the derivative is carried out at fixed  $x_i$  values (Haensel et al. 2002). Clearly, in this case the elastic response of the star will be different from the previous case since matter does not have enough time to reach the complete thermodynamic equilibrium in the meanwhile stresses build-up. This is a well-known problem, already discussed in many papers involving stellar pulsations (Meltzer & Thorne 1966; Channugam 1977; Gourgoulhon et al. 1995; Haensel et al. 2002). Note that the adiabatic index  $\gamma$  is linked to the elastic modulus  $\kappa$  by the relation

$$\kappa = \gamma P. \quad (28)$$

In addition to the equilibrium and frozen adiabatic indexes we introduce also the concept of *effective* adiabatic index: let us consider the initial density

$$\rho_0 = \rho_0(P_0, s_0, x_i), \quad (29)$$

as function of the initial pressure  $P_0$ , entropy  $s_0$  and the set of chemical fractions  $x_i$ . The gradient of (29) is

$$\nabla \rho_0 = \left[ \frac{\partial \rho_0}{\partial P_0} \Big|_{s_0, x_i} \partial_r P_0 + \frac{\partial \rho_0}{\partial s_0} \Big|_{P_0, x_i} \partial_r s_0 + \frac{\partial \rho_0}{\partial x_i} \Big|_{P_0, s_0} \partial_r x_i \right] \mathbf{e}_r, \quad (30)$$

where we used the spherical symmetry of the unperturbed configuration. Using equations (7) and (26) we can recast Eq (30) as

$$\partial_r \rho_0 = - \frac{\rho_0^2 g}{P_0} \left( \frac{1}{\gamma_{eq}} - \frac{1}{\delta \gamma} \right) = - \frac{\rho_0^2 g}{\gamma P_0}. \quad (31)$$

where we have underlined the presence of  $\gamma_{eq}$  plus a departure  $\delta \gamma$ . This equation is an implicit definition of the *effective* adiabatic index  $\gamma$

$$\gamma = - \frac{\rho_0^2 g}{P \partial_r \rho_0}. \quad (32)$$

<sup>3</sup> In other words,  $\gamma_{eq}$  is the index that correctly describes perturbations to the reference configuration when the typical timescale of the dynamical process considered is orders of magnitude larger than that of all the relevant nuclear reactions.



The first term in the RHS of Eq (31) shows how the initial density profile of the star is characterized by a given adiabatic index: a finite value of  $\gamma_{eq}$  yields a negative density gradient  $\partial_r \rho_0$  so that the initial density increases with depth, accordingly to compression of the NS due to its own weight (self-compression). The second term, on the other hand, represents the departure from the self-compression due to non-adiabatic and chemically heterogeneous stratifications. We call *compressional* a stratification that is adiabatic and chemically homogeneous (Cambiotti & Sabadini 2010; Cambiotti et al. 2013).

Once we have chosen a specific EoS, we calculate the initial unstressed configuration in a Newtonian framework, obtaining the radial profiles  $P(r)$  and  $\rho(r)$  via Eqs (7) and (8). In this state the pressure-density relation supporting the star is characterized by the equilibrium adiabatic-index of Eq (26). However, once the loads and rotation are turned on, the response of the star will depend on the dynamical timescale proper of each external force: only in the case of a very slow evolution of the stresses it is possible to use  $\gamma_{eq}$ . In this sense we characterize the initial unstressed configuration by the equilibrium adiabatic index, while the choice of  $\gamma_f$  or  $\gamma_{eq}$  will be used to describe different astrophysical scenarios, depending only on the star's response to external forces.

In this work, in order to maintain consistence with our Newtonian analysis and to study rigorously the importance of possible deviations of the adiabatic index from the value  $\gamma_{eq}$ , we use a polytropic EoS with polytropic index  $n = 1$ , as done, as example in Ushomirsky et al. (2000) and Haskell et al. (2006),

$$P(\rho) = K\rho^2 = Km_n^2 n_b^2, \quad (33)$$

so that the adiabatic index is not a function of the density  $n_b$ , but takes a constant value

$$\gamma_{eq} = \frac{\rho}{K\rho^2} \frac{\partial(K\rho^2)}{\partial\rho} = 2. \quad (34)$$

On the other hand, we have little clues about the actual value of the frozen adiabatic index: typically  $\gamma_f$  is larger than  $\gamma_{eq}$  (Meltzer & Thorne 1966; Channugam 1977; Haensel et al. 2002; Ushomirsky et al. 2000), but the actual relation between them strongly depends on the microscopic model underlying the specific EoS. However, from the practical point of view, the uncertain value of  $\gamma_f$  is not a strong limitation: we will assume different values and study how the estimated stress and strain change, starting from values that differ by only some percent from  $\gamma_{eq}$ , up to the incompressible limit, namely  $\gamma_f \gg \gamma_{eq}$ . Since for most of the EoSs the main difference between the equilibrium and the frozen adiabatic index are expected to be in the crust (Ushomirsky et al. 2000), we choose to change the value of  $\gamma$  only in the elastic layer.

We stress that for any realistic EoS,  $\gamma_{eq}$  and  $\gamma_f$  have a complex dependence on the local properties of matter (see e.g. Douchin & Haensel 2001; Haensel et al. 2002). However, since equilibrium adiabatic index given by Eq (34) is constant, we will assume a constant  $\gamma_f$  in the elastic layer as well.

### 3.1 Strain angle

The strain tensor is obtained from the displacement field via (Landau & Lifshitz 1970)

$$\sigma_{ij} = \frac{1}{2} \left( \frac{\partial u_i}{\partial x_j} + \frac{\partial u_j}{\partial x_i} \right). \quad (35)$$

In order to study the breaking of the elastic crust a failure criterion is needed. We assume the widely used Tresca failure criterion: we thus introduce the *strain angle*, a local quantity  $\alpha(r, \theta)$  that is the difference between the maximum and minimum eigenvalues of the strain tensor at a specific point. The Tresca criterion assumes that, locally, the elastic behavior of a material ceases when the strain angle approaches a particular threshold value  $\sigma^{Max}$ , known as the *breaking strain*

$$\alpha \approx \frac{1}{2} \sigma^{Max}. \quad (36)$$

To date only order-of-magnitude estimates exist for the breaking strain; hence, the particular failure criterion assumed is of secondary importance<sup>4</sup>.

The molecular dynamics simulations performed by Horowitz & Kadau (2009) suggest that  $\sigma_{Max} \sim 10^{-1}$  for a drop of nuclear matter. Using a completely different approach, Baiko & Chugunov (2018) recently found that the maximum strain for a polycrystalline crust is  $\sim 0.04$ . On the other hand, Ruderman (1991b) reasoned that, if crust has already undergone many cracks events, a macroscopic estimate for  $\sigma^{Max}$  should be in the range  $10^{-5} \div 10^{-3}$ . Hence, to take into account for the large uncertainties on the breaking strain, we will consider constant values of  $\sigma^{Max}$  in the whole range  $10^{-5} \div 10^{-1}$ .

## 4 BOUNDARY CONDITIONS

In order to solve Eq (23) we have to impose some boundary conditions. Firstly, we assume that the material does not cross the interface between two elastic layers. Secondly, all the spheroidal vector solutions are continuous across the boundaries between different layers, say at  $r = r_j$ , so that (Sabadini et al. 2016)

$$\mathbf{y}_{\ell m}(r_j^-) = \mathbf{y}_{\ell m}(r_j^+). \quad (37)$$

This continuity requirement gives us a straightforward way to impose simply boundary conditions at the surface and at the core-crust boundary.

### 4.1 Surface-vacuum boundary

Let  $a$  be the stellar radius. The behaviour of the spheroidal solution at the boundaries suggests us three simple conditions. The first is that the potential stress (22) must be continuous across the interface at  $r = a$ , i.e.

$$Q_{\ell m}(a^-) = Q_{\ell m}(a^+). \quad (38)$$

<sup>4</sup> An alternative could be the Von Mises criterion, adopted e.g. by Lander et al. (2015) and Ushomirsky et al. (2000)

To implement the condition (38) in our model, let us first expand the centrifugal potential as

$$\phi^C(r, \theta, \varphi) = \phi_{00}^C(r) Y_{00}(\theta, \varphi) + \sum_{m=-2}^2 \phi_{2m}^C(r) Y_{2m}(\theta, \varphi), \quad (39)$$

where

$$\phi_{00}^C(r) = -\frac{\Omega^2 r^2}{3} \quad (40)$$

and

$$\phi_{2m}^C(r) = \frac{\Omega^2 r^2}{3} \frac{(2-m)!}{(2+m)!} Y_{2m}(\theta, \varphi), \quad (41)$$

while the other harmonic coefficients of the expansion being zero:

$$\phi_{\ell m}^C = 0 \quad \text{for } \ell = 1, 3, \dots \infty. \quad (42)$$

Neglecting for the moment the  $\ell = 0$  term, we can assume

$$\phi_{\ell m}^C(r) = \phi_{\ell m}^C(a) \left(\frac{r}{a}\right)^\ell. \quad (43)$$

The expansion of the gravitational and tidal potential is easy, since the Poisson equation (14) reduces to the Laplace equation in the region between the NS and the body exerting the tidal force, placed at radius  $a^T$ . By imposing the regularity conditions for  $r \rightarrow \infty$  and  $r \rightarrow 0$ , we obtain

$$\phi_{\ell m}^\Delta(r) = \phi_{\ell m}^\Delta(a) \left(\frac{r}{a}\right)^{-\ell-1} \quad r > a \quad (44)$$

$$\phi_{\ell m}^T(r) = \phi_{\ell m}^T(a) \left(\frac{r}{a}\right)^\ell \quad r < a^T. \quad (45)$$

Thanks to the expansions in Eqs (43, 44, 45), we obtain the general form of the expression in Eq (38) as

$$Q_{\ell m}(a^-) = \frac{2\ell+1}{a} \left[ \phi_{\ell m}^C(a^+) + \phi_{\ell m}^T(a^+) \right]. \quad (46)$$

Note that the terms due to the gravitational potential do not appear in the right hand side of the above equation: they cancel each other as can be seen by using Eq (44),

$$\partial_r \phi_{\ell m}^\Delta(a^+) = -\frac{\ell+1}{a} \phi_{\ell m}^\Delta(a). \quad (47)$$

Besides Eq (46), we impose that the tangential stress  $S_{\ell m}$  must be zero in vacuum,

$$S_{\ell m}(a^+) = 0. \quad (48)$$

The same is valid for the radial stress  $R_{\ell m}$  since the pressure outside the star is zero,

$$R_{\ell m}(a^-) = 0. \quad (49)$$

The three conditions (46, 48, 49) can be rearranged in the compact form

$$\mathbf{P}_1 \mathbf{y}(a^-) = \mathbf{b} \quad (50)$$

where  $\mathbf{P}_1$  is a projector that selects only the third, fourth and sixth components of the spheroidal vector solution  $\mathbf{y}$  and the vector  $\mathbf{b}$  is defined as

$$\mathbf{b} = \begin{pmatrix} 0 \\ 0 \\ -\frac{(2\ell+1)}{a} (\phi_{\ell m}^C + \phi_{\ell m}^T) \end{pmatrix}. \quad (51)$$

## 4.2 Core-Crust boundary

In our model the core is fluid and inviscid, so that it cannot support deviatoric stresses. Also across the core-crust boundary we can use the continuity of the spheroidal vector but, differently with respect to the previous case, we have to allow for a free slip at the interface (i.e. the core can slip under the crust). This request implies that

$$\mathbf{y}(r_c^+) = \begin{pmatrix} U_{\ell m}(r_c^-) \\ 0 \\ R_{\ell m}(r_c^-) \\ 0 \\ \Phi_{\ell m}(r_c^-) \\ Q_{\ell m}(r_c^-) \end{pmatrix} + \begin{pmatrix} 0 \\ C_2 \\ 0 \\ 0 \\ 0 \\ 0 \end{pmatrix}, \quad (52)$$

where  $r_c$  is the core-crust radius and  $C_2$  is a constant of integration describing the tangential displacement. The vector solution in the core can be easily found; by setting  $\mu = 0$  and omitting the terms related to the loading of the crust, Eqs (15) and (16) can be rearranged as

$$\frac{\partial_r R_{\ell m}}{\rho_0} - \partial_r (g U_{\ell m}) + g \chi_{\ell m} - \partial_r \Phi_{\ell m} = 0 \quad (53)$$

$$\frac{R_{\ell m}}{\rho_0} - g U_{\ell m} - \Phi_{\ell m} = 0. \quad (54)$$

By using these two equations into the Poisson one (19), we obtain

$$\nabla_r^2 \Phi_{\ell m} = 4\pi G \partial_r \rho_0 \frac{\Phi_{\ell m}}{g}. \quad (55)$$

Since  $\partial_r \rho_0 = 0$  must hold at the center of the star, the regularity of the potential in  $r = 0$  implies

$$\lim_{r \rightarrow 0} r^\ell \psi_{\ell m}(r) = 1, \quad (56)$$

with  $\Phi_{\ell m}(r) = C_1 \psi_{\ell m}(r)$ . This proportionality relation will be particularly convenient and useful in the following calculation.

Subtracting the radial derivative of Eq (54) from (53), and using the relation

$$R_{\ell m} = \kappa \chi_{\ell m}, \quad (57)$$

valid in the fluid limit, we obtain the so-called Adams-Williamson relation (Cambiotti & Sabadini 2010; Cambiotti et al. 2013),

$$\frac{\kappa}{\rho_0^2} \left( \partial_r \rho_0 + \frac{\rho_0^2 g}{\gamma P} \right) \chi_{\ell m} = 0, \quad (58)$$

that can be equivalently written using Eq (31), as

$$\frac{\kappa}{\rho_0^2} \frac{\partial_r \rho_0}{\gamma} (\gamma - \gamma_{eq}) \chi_{\ell m} = 0. \quad (59)$$

Clearly, when the stratification is compressional (i.e.  $\gamma = \gamma_{eq}$ , see section 3), the above equation is automatically satisfied. This case is of interest for the study of a neutron star that gradually changes its state of rotation: the dynamical timescales of both spin-up or spin-down are large enough to allow for an elastic response at chemical equilibrium. Therefore, the two Eqs (53) and (54) are not linearly independent, providing a way to constrain the radial stress at the core-crust interface:

$$R_{\ell m} = \rho_0 g \left[ U_{\ell m} - \left( -\frac{\Phi_{\ell m}}{g} \right) \right] = \rho_0 g C_3, \quad (60)$$

where the constant of integration  $C_3$  indicates the difference between the radial displacement  $U_{\ell m}$  and the geoid displacement at  $r = r_c$

$$U_{\ell m}^{\text{geoid}} = -\frac{\Phi_{\ell m}(r)}{g(r)}. \quad (61)$$

Note that in the case of compressional stratification the volume change within the core is undetermined: below the core-crust interface we cannot specify the displacement and radial stresses with the above assumptions. However, this does not constitute a problem because we are interested only in the deformation of the crust, which is uniquely determined by the boundary conditions. The constants  $C_1, C_2, C_3$  define the boundary solution of the core, that can be written as

$$\mathbf{y}_{\ell m}^{\text{core}}(r_c) = \begin{pmatrix} -C_1 + \frac{\psi_{\ell m}}{g} + C_3 \\ C_2 \\ \rho_0 g C_3 \\ 0 \\ C_1 \psi_{\ell m} \\ C_1 q_{\ell m} + 4\pi G \rho_0 C_3 \end{pmatrix}, \quad (62)$$

where we have defined

$$q_{\ell m} = \partial_r \psi_{\ell m} + \frac{\ell+1}{r} \psi_{\ell m} - \frac{4\pi G}{g} \psi_{\ell m}. \quad (63)$$

The core-crust boundary condition (52) can thus be written in the compact form

$$\mathbf{y}_{\ell m}(r_c^+) = \mathbf{I}_C \mathbf{C}, \quad (64)$$

where  $\mathbf{I}_C$  is the  $6 \times 3$  matrix

$$\mathbf{I}_C = \begin{pmatrix} -\psi_{\ell}(r_c)/g(r_c) & 0 & 1 \\ 0 & 1 & 0 \\ 0 & 0 & g(r_c)\rho_0(r_c^-) \\ 0 & 0 & 0 \\ \psi_{\ell}(r_c) & 0 & 0 \\ q_{\ell}(r_c) & 0 & 4\pi G \rho_0(r_c^-) \end{pmatrix} \quad (65)$$

and  $\mathbf{C}$  is the 3-vector

$$\mathbf{C} = (C_1, C_2, C_3). \quad (66)$$

### 4.3 Elastic solution

The general solution of the differential system (23) reads

$$\mathbf{y}_{\ell m}(r) = \mathbf{\Pi}_{\ell}(r, r_0) \mathbf{y}_0 - \int_{r_0}^r \mathbf{\Pi}_{\ell m}(r, r') \mathbf{h}_{\ell m}(r') dr', \quad (67)$$

where  $\mathbf{y}_0$  is just a shorthand notation for  $\mathbf{y}_{\ell m}(r_0)$ . The first terms on the right side of Eq (67) is the homogeneous solution, while the second term is a particular solution which accounts for the external non-conservative forces. The so-called *propagator* matrix  $\mathbf{\Pi}_{\ell m}$  solves the homogeneous equation

$$\frac{d\mathbf{\Pi}_{\ell}(r, r')}{dr} = \mathbf{A}_{\ell}(r) \mathbf{\Pi}_{\ell}(r, r'), \quad (68)$$

with the condition

$$\mathbf{\Pi}_{\ell}(r', r') = \mathbf{1}. \quad (69)$$

Moreover, at every boundary we impose the continuity of the propagator

$$\mathbf{\Pi}_{\ell}(r_j^+, r') = \mathbf{\Pi}_{\ell}(r_j^-, r'). \quad (70)$$

If we choose the core-crust radius as the starting point of the integration, namely  $r_0 = r_c^+$ , we have

$$\mathbf{y}_{\ell m}(r_c^+) = \mathbf{y}_0 = \mathbf{I}_C \mathbf{C}. \quad (71)$$

This gives us

$$\mathbf{y}_{\ell m}(r) = \mathbf{\Pi}_{\ell}(r, r_c^+) \mathbf{I}_C \mathbf{C} - \mathbf{w}(r), \quad (72)$$

where  $\mathbf{w}(r)$  is defined as

$$\mathbf{w}(r) = \int_{r_c^+}^r \mathbf{\Pi}_{\ell}(r, r') \mathbf{h}_{\ell m}(r') dr'. \quad (73)$$

The three constants of integration in the vector  $\mathbf{C}$  can be estimated by imposing the conditions at the star surface via Eq (50), so that Eq (72) now reads

$$\mathbf{y}_{\ell m}(r) = \mathbf{\Pi}_{\ell}(r, r_c) \mathbf{I}_C [\mathbf{P}_1 \mathbf{\Pi}_{\ell}(a^-, r_c^+) \mathbf{I}_C]^{-1} (\mathbf{P}_1 \mathbf{w}(a^-) + \mathbf{b}) - \mathbf{w}(r). \quad (74)$$

This equation represents the response of the star to the internal and centrifugal loads: it uniquely determines the spheroidal deformations and the potential within the crust, as well as the radial and tangential spheroidal stresses and the potential stress. Vortex pinning in the crust is an example of non-conservative loading force that can stress the crust and can be encoded into the term  $\mathbf{w}(r)$ . In our explicit case of study, the only external force is conservative (the centrifugal force): in this case the solution in Eq (67) assumes the simpler form

$$\mathbf{y}_{\ell m}(r) = \mathbf{\Pi}_{\ell}(r, r_c) \mathbf{I}_C [\mathbf{P}_1 \mathbf{\Pi}_{\ell}(a^-, r_c^+) \mathbf{I}_C]^{-1} \mathbf{b}. \quad (75)$$

Moreover, when deformations with respect to the spherical reference configuration are induced only by rotation, the displacement field  $\mathbf{u}$  is the sum of only two contributions, namely  $\mathbf{u} = \mathbf{u}_{00} + \mathbf{u}_{20}$ . This decomposition relies on the fact that we have assumed a constant rotation axis; taking into account also a possible nutation would in general require the contributions of other  $m \neq 0$  harmonics.

## 5 NUMERICAL SOLUTION FOR THE POLYTROPE $n = 1$

As anticipated in section 3, we will study the behaviour of a neutron star described by a polytrope with  $n = 1$ . In particular, we are interested in the comparison of displacements and strains of neutron stars with different masses. However, the  $n = 1$  polytrope has a degenerate mass-radius relation, in the sense the radius  $a$  and the mass  $M$  are independent of one another. Hence, we fix the relation  $a(M)$  by considering the SLy equation of state (Douchin & Haensel 2001) and solving the Tolman-Oppenheimer-Volkoff equations (TOV), see Fig 2. Despite the fact that the description of the star is made in a Newtonian framework, the mass-radius relation of the reference configuration is the one obtained in General Relativity. This is nothing but a prescription to fix the mass and radius of our polytropic star and, at the same time, gives us realistic values of the radius, implying reasonable estimates of the centrifugal force, as already done in Gilierti et al. (2018).

For a given mass  $M$  in the range  $1M_{\odot} \div 2M_{\odot}$  we can

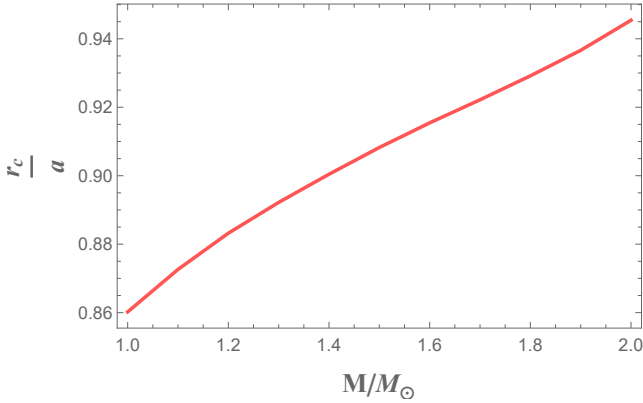


**Figure 2.** Normalized core-crust radius  $r_c/a$  as a function of the stellar mass, obtained for the SLy EoS.

calculate the corresponding value of  $K$  in Eq (33) and of the central density  $\rho_{ce} = \rho(r=0)$  as

$$K = \frac{2}{\pi} a^2 G$$

$$\rho_{ce} = \frac{M}{4\pi^2} \left( \frac{K}{2\pi G} \right)^{-3/2}.$$

The crust-core transition is set at the fiducial density  $1.5 \times 10^{14} \text{ g/cm}^3$ , that imply a core-crust transition at  $r_c \approx 0.90 a$  for a standard neutron star with  $M = 1.4 M_\odot$ .

Following Ushomirsky et al. (2000), the outer-crust boundary is placed at the density  $1 \times 10^{11} \text{ g/cm}^3$  in order to guarantee the numerical stability of the solution against the computational problems due to the very rapid variation of the density in the outermost layers. Since the outer crust represents only a negligible fraction of the stellar mass, this truncation is not expected to have a severe impact on our numerical calculations.

### 5.1 Slow dynamics

The elastic response of the star is fixed by the EoS and by the poorly known parameters  $\kappa$  and  $\mu$  in the crust. For  $\kappa$  we choose at first the equilibrium bulk modulus, given by (28)

$$\kappa(r) = \gamma_{eq} P(r). \quad (76)$$

With this choice we are implicitly assuming that the stellar evolution has a much longer timescale compared to the one of the chemical reactions near equilibrium.

For the shear modulus we follow the same prescription guessed by Cutler et al. (2003),

$$\mu(r) = 10^{-2} \times P(r). \quad (77)$$

All the physical quantities in our code are normalized by using the stellar radius  $a$ , the central density  $\rho_{ce}$ , the typical shear modulus  $\mu_c$  at the core-crust interface  $r_c$  and the angular velocity  $\Omega$  of the particular NS under consideration. The first two parameters vary with  $M$ , while the other two are fixed. In Tab 1 we report some values for a  $M = 1.4 M_\odot$  neutron star. In the following we show the results for a NS having the values reported in Tab 1, if not otherwise stated.

The EoS, the adiabatic index governing perturbations, the shear modulus and the boundary densities which define

**Table 1.** Parameters for a typical neutron star with  $M = 1.4 M_\odot$ , as considered in this work. The angular velocity is set to the reference value 1 rad/s, so that the our numerical results can be easily rescaled to the case of different angular velocities.

$a$ (cm)	$\rho_{ce}(\text{g/cm}^3)$	$\mu_c(\text{dyn/cm}^2)$	$\Omega(\text{rad/s})$
$1.17 \times 10^6$	$1.38 \times 10^{15}$	$10^{30}$	1

the layers completely fix the elastic behaviour of the star: we can now study the effects of the centrifugal force, starting from a non-rotating and unstressed reference configuration.

The centrifugal potential is particular as its expansion consists of only two spherical harmonics having  $m = 0$ , one with  $\ell = 0$  and another one with  $\ell = 2$ . In the following we will show the displacements and strains due to each of these contributions separately; the total effect of rotation is given by the sum of the two.

In Fig 3 the radial and tangential displacements are shown for the harmonic  $\ell = 2$ , while the harmonic term  $\ell = 0$  is presented in Fig 4. In both cases the units have been normalized: in order to get the dimensional quantities for a given angular velocity  $\Omega$ , it is necessary to multiply these functions by the dimensionless factor

$$d(\Omega) = \frac{1}{3} \frac{\Omega^2 a^2}{v^2}, \quad (78)$$

where  $v$  is a velocity defined as  $v = \sqrt{\mu_c/\rho_{ce}}$ . To be more explicit, the results must be rescaled as

$$\mathbf{y} = d(\Omega) \times \begin{pmatrix} a \\ a \\ \mu_c \\ \mu_c \\ v^2 \\ v^2/a \end{pmatrix} \tilde{\mathbf{y}}, \quad (79)$$

where the tilde superscript indicates the dimensionless quantities. For practical purposes one can use the expression

$$d(\Omega) = 6.2 \times 10^{-4} \left( \frac{\Omega}{1 \text{ rad/s}} \right)^2 \left( \frac{\rho_{ce}}{1.38 \times 10^{15} \text{ g/cm}^3} \right) \times \left( \frac{\mu_c}{10^{30} \text{ dyn/cm}^2} \right)^{-1} \left( \frac{a}{1.167 \times 10^6 \text{ cm}} \right)^2, \quad (80)$$

calculated by using a  $M = 1.4 M_\odot$  neutron star as a reference. According to our model and with the parameters given in Table 1, the displacement with respect to the non-rotating configuration is of the order of  $|u_r(a)| \simeq 4.2 \times 10^{-3} \text{ cm}$  at the equator. As we can see, the harmonic degree  $\ell = 0$  gives a smaller contribution to the total displacement if compared to the  $\ell = 2$  contribution as we find that  $2.5 \leq |U_{20}/U_{00}| \leq 2.9$ . Note that the  $\ell = 0$  contribution corresponds to a global increase of volume of the star, since it is positive at every latitude.

Let's now explore the possibility of crust failure, by calculating the strain angle  $\alpha$  and using the Tresca criterion in Eq (36). Our analysis shows that:

(i) In Fig 5, the normalized strain angle  $\tilde{\alpha} = \alpha/d(\Omega)$  is shown as a function of the colatitude  $\theta$  and of the normalized radius  $r/a$ . We see that the strain angle is an increasing function of the radius, contrary to the uniform, incompressible case studied by Franco et al. (2000) and Giliberti et al.



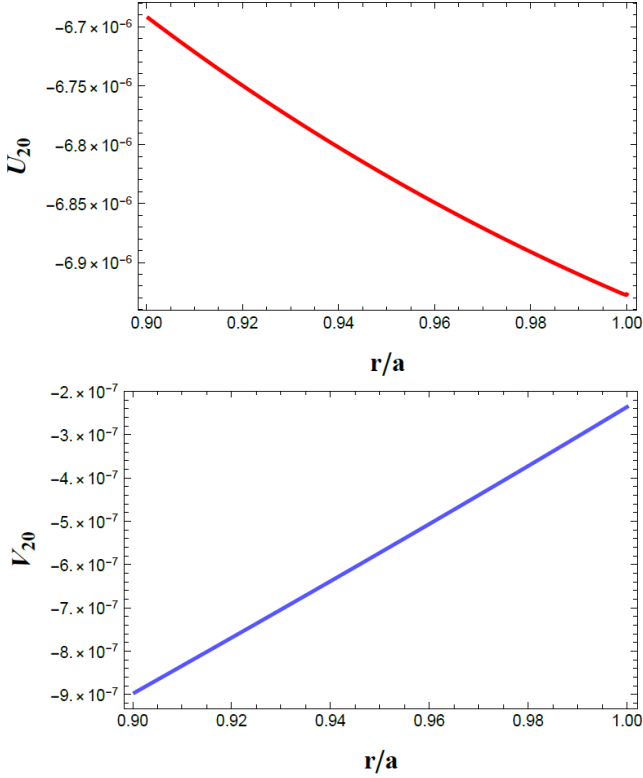


**Figure 3.** The  $U_{20}(r)$  (top) and the  $V_{20}(r)$  (bottom) normalized displacements as functions of the normalized radius, from  $r = r_c$  to  $r = a$ .

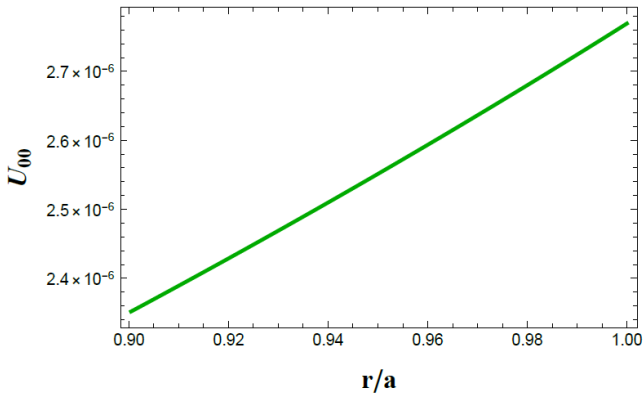


**Figure 4.** The  $U_{00}(r)$  normalized displacement as a function of the normalized radius, from  $r = r_c$  to  $r = a$ .

(2018). This was already noticed by Cutler et al. (2003): in the present model the shear modulus is not a constant but a decreasing function of the stellar radius, implying that the strain is expected to be larger near the surface.

(ii) Differently from the incompressible and uniform model of Franco et al. (2000), where the strain maximum is at the equator, in the case discussed here we find that the maximum value of the strain angle  $\alpha^{Max}$  occurs at the poles.

(iii) For what concerns the dependence on mass,  $\alpha$  is a decreasing function of  $M$ , as can be seen in Fig 6, where we

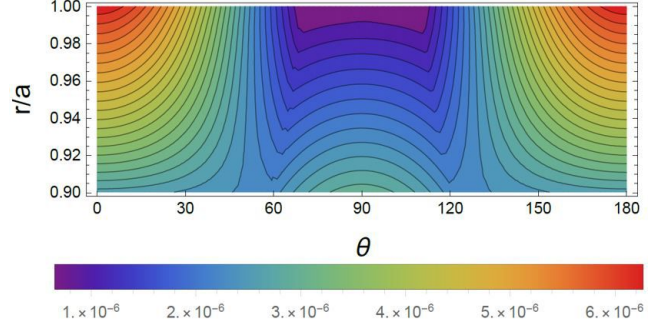


**Figure 5.** Color map of the normalized strain angle  $\alpha$  as a function of the colatitude and of the normalized radius  $r/a$ . The region shown here refers to the crustal layer, from  $r = r_c$  to  $r = a$  for a  $M = 1.4M_\odot$  NS.

calculated the parameter  $d$  defined in (78) for the benchmark value  $\Omega = 1$  rad/s. This behaviour can be understood in the incompressible limit of our model by considering a uniform elastic star, namely a star with only one uniform elastic layer extending from the center to the crust, as in Baym & Pines (1971). For this simplified model, the displacement  $\mathbf{u}$  turns out to be (Love 1934)

$$\begin{aligned} u_r &= W \left[ r \left( \frac{r^2}{a^2} - \frac{8}{3} \right) \right] P_2(\theta) \\ u_\theta &= W \left[ r \left( 8 - 5 \frac{r^2}{a^2} \right) \right] \frac{dP_2}{d\theta}(\theta), \end{aligned}$$

where the dimensionless factor

$$W = \frac{\Omega^2 a^2}{v_K^2} \quad (81)$$

is the ratio between the squared equatorial velocity  $\Omega^2 a^2$  and the Keplerian one  $v_K = \sqrt{GM/a}$ . The key factor for the global behaviour of  $\alpha$  is hidden into the factor  $W$ , which turns out to be proportional to

$$W \propto \frac{a^3}{GM} \propto \frac{1}{\rho}. \quad (82)$$

Therefore, for more massive (i.e. denser) stars, smaller displacements are expected. This reasonable behaviour, which appears as a by-product of the simplified models of Franco et al. (2000) or Giliberti et al. (2018) seems also to be a typical feature of more refined models, as can be seen in Fig 6. Unfortunately, it is more difficult<sup>5</sup> to justify this behavior with an analytical argument by using models that go beyond the incompressible one presented in Giliberti et al. (2018).

(iv) The strain have a slightly larger slope as a function of  $M$  if we compare the homogeneous and the compressible models. In the first case, the ratio between the maximum strain angle  $\alpha$  calculated for a  $M = 1 M_\odot$  and for  $M = 2 M_\odot$  is about  $2 \div 3$ , depending on the EoSs used (Giliberti et al. 2018), while in the compressible case we have

$$\frac{\alpha^{Max}(M = 1M_\odot)}{\alpha^{Max}(M = 2M_\odot)} \simeq 4. \quad (83)$$

<sup>5</sup> The difficulty stems from the fact that if the star is incompressible, like in the model of Giliberti et al. (2018), we have only the contribution due to the  $\ell = 2$  harmonic, while in our model also the effect of the  $\ell = 0$  mode is present.

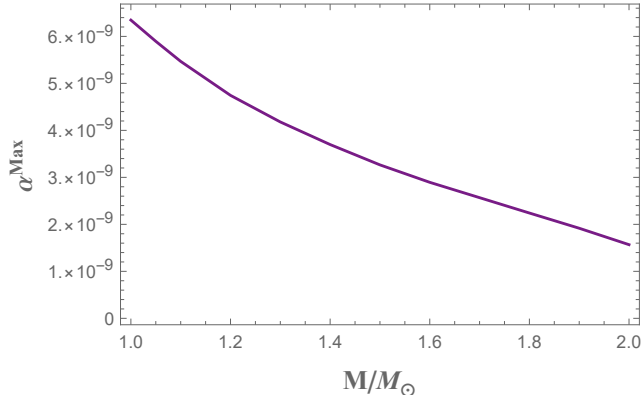


**Figure 6.** The maximum strain angle as a function of the mass, assuming  $\gamma = \gamma_{eq}$  and  $\Omega = 1$  rad/s.

In this sense, we expect the strain angle to have a stronger dependence on the stellar mass in refined and realistic models with respect to what is found by employing an homogeneous model.

## 5.2 Fast dynamics

We want now to explore a different scenario, assuming that the dynamical timescale of the perturbations is fast with respect to the reactions ones. This can be done by using the frozen adiabatic index instead of the equilibrium one, i.e.

$$\kappa(r) = \gamma_f P(r). \quad (84)$$

Since the polytropic EoS that we employ does not have a typical value for the non-equilibrium adiabatic index, we make a comparison between different values of  $\gamma_f$ . This allows us to study how the adiabatic index value changes the star's response to the same external centrifugal force: we compare the displacements, stresses and strains in four different cases, characterized by the adiabatic indexes  $\gamma_1 = 2$ ,  $\gamma_2 = 2.1$ ,  $\gamma_3 = 200$  and  $\gamma_4 = \infty$ . The value of  $\gamma_2$  is 5% larger than the equilibrium adiabatic index, while  $\gamma_3$  mimics a very strong departure from the equilibrium, towards the incompressible limit  $\gamma \rightarrow \infty$ ; actually, we expect the same stellar response for  $\gamma_3$  and  $\gamma_4$ , since the first is just a numerical counterpart of the analytical incompressible limit.

Although the analysis is similar to the one carried out in previous section, a remark on the Adams-Williamson equation is due in this case. Since in a neutron star it is expected that (Chamel & Haensel 2008)

$$\frac{\mu}{\kappa} \ll 1, \quad (85)$$

the key physical aspects of the problem are already present by studying in the  $\mu \rightarrow 0$  limit. Therefore, we can consider the equations (15) and (16) in the reduced form given in Eqs (53) and (54), obtaining Eq (31). Now, if  $\gamma \neq \gamma_{eq}$  the Adams-Williamson equation (31) requires  $\chi_{\ell m}$  to be zero, implying that there can be no volume changes, see Eq (18). Therefore,

$$R_{\ell m} = \kappa \chi_{\ell m} = 0, \quad (86)$$

and via (54) it is possible to show that the radial displacement must coincide with the geoid perturbation defined in

(61). As a check, let us focus on the  $\ell = 2$  harmonic contribution by studying the radial displacement  $U_{20}$  and the geoid radial displacement introduced in Eq (61): in Fig 7 it is shown that the cases  $\gamma_f = 200$  and  $\gamma_f = \infty$  give in practice the same results.

For the shear modulus provided in Eq (77), the difference between the radial and the geoid displacements decreases by increasing the adiabatic index: in the  $\gamma_f = \gamma_{eq}$  case (panel-a of Fig 7) we have a clear departure from the geoid, but if  $\gamma_f = 200$  the two radial displacement almost coincide.

As a further step towards a better understanding of the response of the star, we calculate the radial and the geoid displacements for  $\gamma_f = 2.1$  but with a shear modulus that is smaller than the one considered in Eq (77). When the elastic shear becomes smaller, the radial  $U_{20}$  displacement and the geoid one become similar, as shown in Fig 8. This expected behaviour has been also discussed in Cambiotti & Sabadini (2010) and Cambiotti et al. (2013) for a viscoelastic Earth model at large time scales (from million to billion years), when the shear stress goes to zero due to stress relaxation by viscous flow (as in the  $\mu \rightarrow 0$  limit).

To properly understand the contribution of the  $\ell = 0$  harmonic we need a further argument. As the out-of-equilibrium adiabatic index value increases, we approach the incompressible limit, which provides a strong bond on the radial displacement. In general  $\chi_{\ell m}$  assumes the form

$$\chi_{\ell m} = \partial_r U_{\ell m} + \frac{2}{r} U_{\ell m} - \frac{\ell(\ell+1)}{r} V_{\ell m}. \quad (87)$$

Since incompressibility requires  $\chi_{\ell m} = 0$ , the above relation becomes (the  $\ell = 0$  displacement is purely radial)

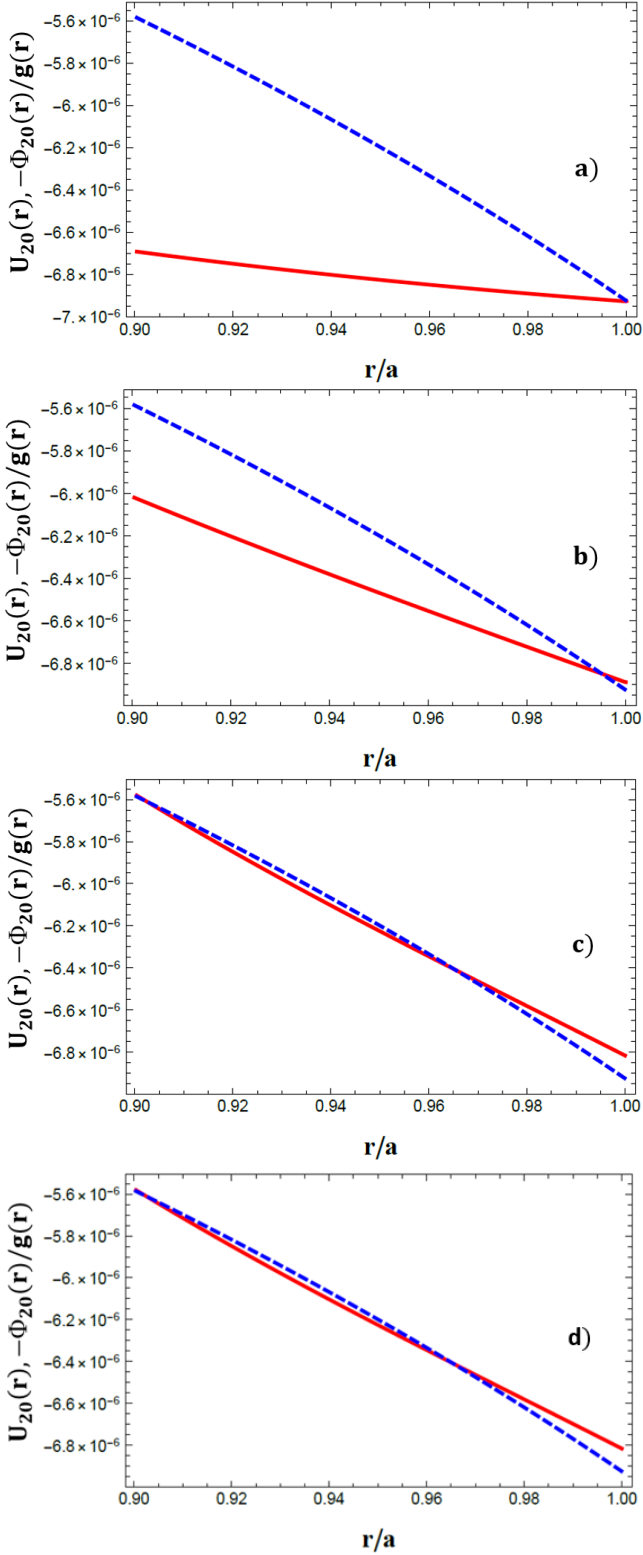
$$\partial_r U_{00} = -2 \frac{U_{00}}{r}. \quad (88)$$

We remind that in our model we vary only the crust adiabatic index, and thus the core maintains its equilibrium compressibility also in the limiting case in which the crust is incompressible. Therefore, also for  $\gamma_f = \infty$  the radial displacement is different from zero because the core modifies its shape during the spin-down, loading the crust. The balance between the core stress and the incompressible relation (88) determines the radial displacement of the  $\ell = 0$  harmonic. In Fig (9) both  $\partial_r U_{00}$  and  $-2U_{00}/r$  are shown for the four different adiabatic indexes considered.

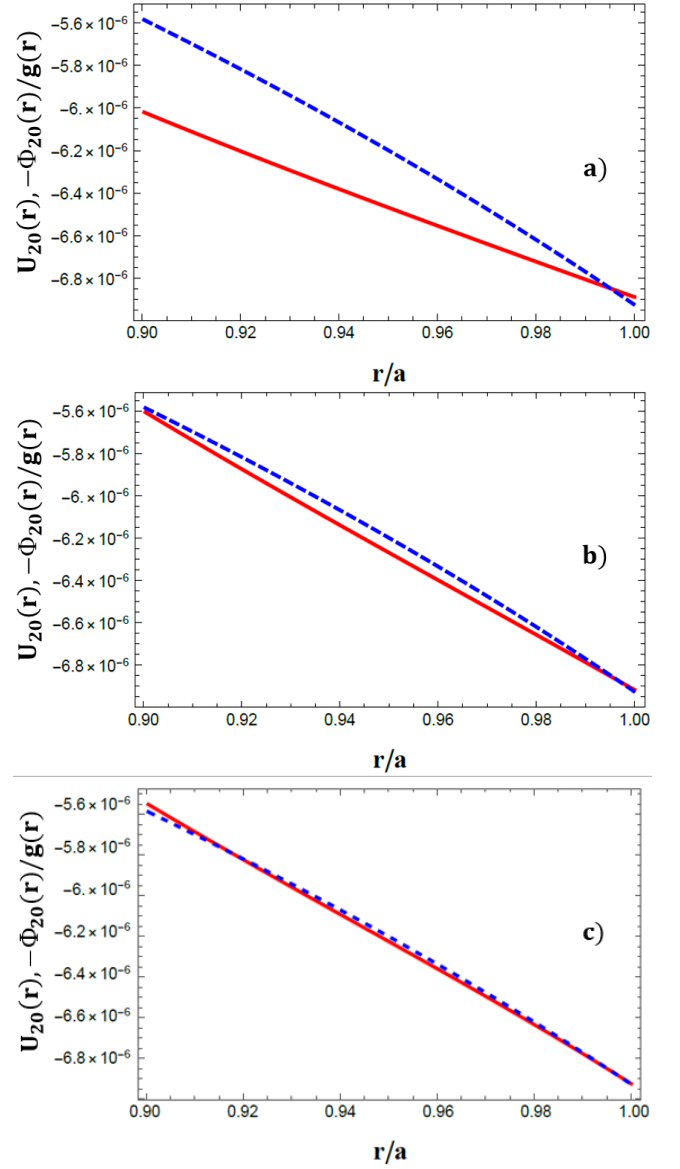
It is interesting to observe that even a small departure from the equilibrium value of the adiabatic index carries the system to a configuration similar to the incompressible one, as can be seen in Figs 10 and 11. Figure 10 shows the normalized values of  $U_{20}$  and  $V_{20}$  for a  $M = 1.4M_\odot$  rotating neutron star, according to the values listed in Tab 1; the response of the star to the same change of the centrifugal force is very different in the equilibrium scenario with respect to the frozen ones. The same consideration is valid for the tangential stress  $S_{\ell m}$ , shown in Fig 11.

Figure 12 shows the radial displacement  $U_{00}$  for the same stellar mass  $M = 1.4M_\odot$ : again we note the difference between the equilibrium scenario and the frozen ones, with the change of the slope of the plotted curve for different  $\gamma$ , as expected from Eq (88). Again,  $U_{00} > 0$  since the star undergoes a global increase of volume due to the effect of rotation.

Furthermore, in Fig 13 we plot the maximum strain



**Figure 7.** Radial  $U_{20}$  (red, solid) and geoid (blue, dashed) normalized displacements as a function of the normalized radius, from  $r = r_c$  to  $r = a$ , for fixed shear modulus  $\mu$  and different values of the adiabatic index:  $\gamma = 2$  (a),  $\gamma = 2.1$  (b),  $\gamma = 200$  (c) and  $\gamma = \infty$  (d). As discussed in the text the incompressible limit  $\gamma = \infty$  gives the same response as the case in which  $\gamma = 200$ .



**Figure 8.** Radial  $U_{20}$  (solid, red) and geoid (blue, dashed) normalized displacements as a function of the normalized radius, from  $r = r_c$  to  $r = a$ , for fixed adiabatic index  $\gamma = 2.1$  and  $\mu = 10^{-2}P$  (a),  $\mu = 10^{-3}P$  (b) and  $\mu = 10^{-4}P$  (c).

angle  $\alpha$  as a function of  $r$  and  $\theta$ . The color maps representing the various values of  $\alpha$  differ significantly when going from the equilibrium to the non-equilibrium configurations. The adiabatic index value influences the slope of the strain angle curve: if for  $\gamma_f = 2$ ,  $\alpha$  is an increasing function of  $r$ , for  $\gamma_f = 2.1, 200, \infty$  the opposite is true, and we recover the incompressible behaviour described in Franco et al. (2000) and Giliberti et al. (2018).

Finally, we try to get a feeling of the impact of the stellar mass parameter  $M$  by studying the function  $\alpha(M)$ . Note that in this case we cannot simply study the normalized strain angle, since also the normalizing factor in (78) depends on the stellar mass through  $a$  and  $v$ . Hence, in order to give a result that can be easily rescaled, we impose  $\Omega = 1$  rad/s. We find that the strain dependence on mass is

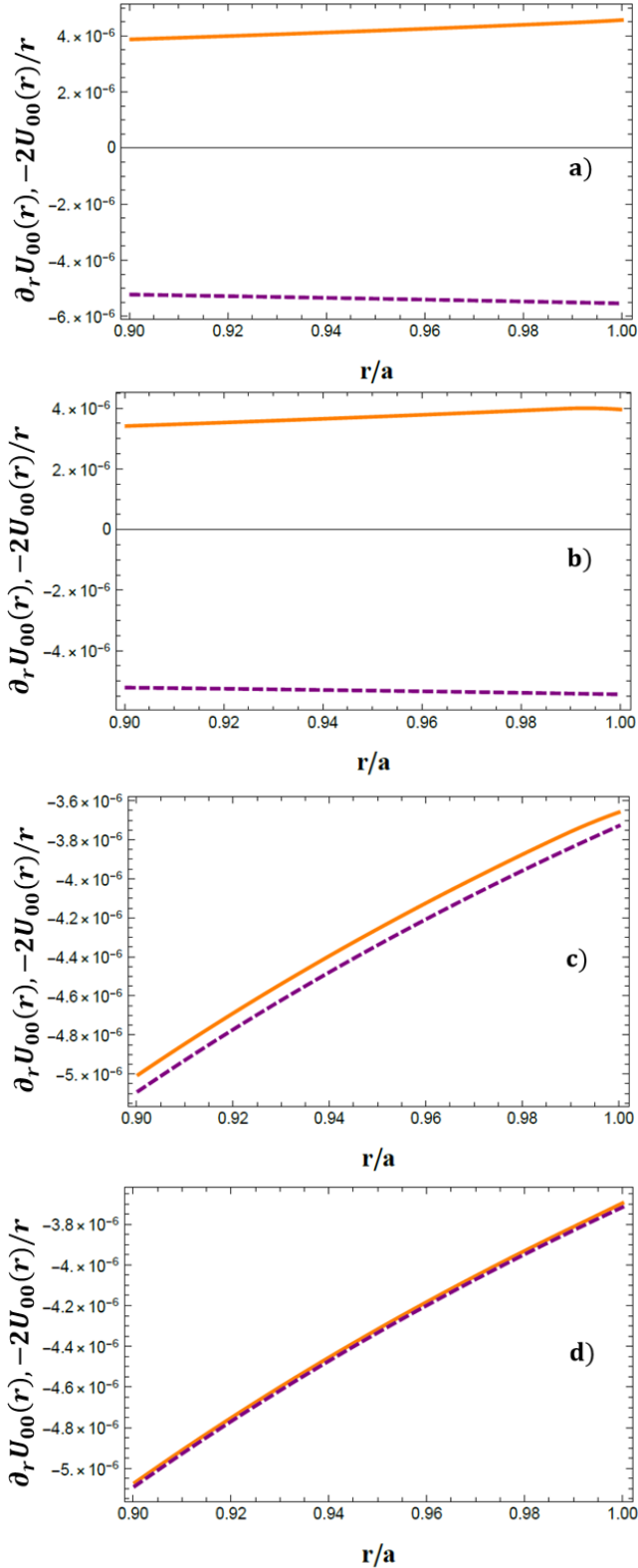


**Figure 9.**  $\partial_r U_{00}$  (orange) and  $-2U_{00}/r$  (purple) calculated for  $\gamma = 2$  (a),  $\gamma = 2.1$  (b),  $\gamma = 200$  (c) and  $\gamma = \infty$  (d).

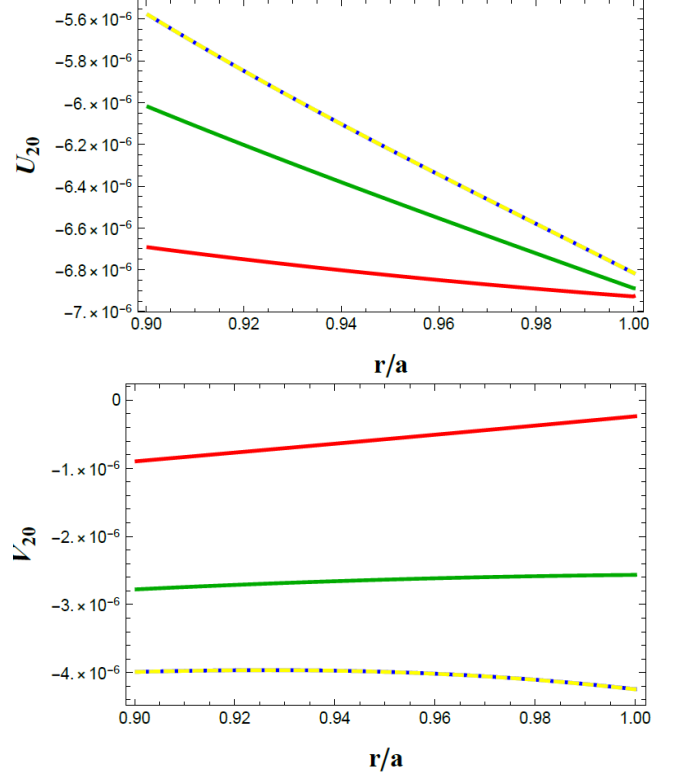


**Figure 10.** Normalized  $U_{20}(r)$  (top) and  $V_{20}(r)$  (bottom) displacements as function of the normalized radius. The plot refers to the crustal region, extending from  $r = r_c$  to  $r = a$ . The same procedure is used with different adiabatic indexes:  $\gamma = 2$  (red),  $\gamma = 2.1$  (green),  $\gamma = 200$  (blue) and  $\gamma = \infty$  (yellow dashed).

almost the same for every value of the frozen adiabatic index. We checked this behaviour by employing a larger set of values for  $\gamma_f$ , with values ranging from  $\gamma_f = 2$  to  $\gamma_f = 1000$ , as reported in Fig 14.

The comparison between different adiabatic indexes allows to calculate the ratio in Eq (83) for different scenarios, going from the equilibrium to the incompressible one. This is shown in Fig 15. As we can see that ratio has large values when values near  $\gamma_{eq}$  are employed, but it rapidly decreases towards the asymptote  $\alpha(1M_\odot)/\alpha(2M_\odot) \simeq 2.6$  as the incompressible limit is approached. This latter value resembles the one obtained with the homogeneous two-density incompressible model where  $\alpha(1M_\odot)/\alpha(2M_\odot) \simeq 2 \div 3$  (Giliberti et al. 2018).

### 5.3 Effective adiabatic index: the effect of General Relativity

We end this section with a technical note, expanding the motivation behind our basic working assumption of a non-relativistic framework.

The Adams-Williamson equation (58) tells us that the adiabatic index (both the equilibrium one as well as the more uncertain frozen one) depends strongly on the stratification: this can be envisaged by comparing the *effective* adiabatic index of Eq (32), calculated by using the equilibrium configuration of a star. As an explicit example we do this for

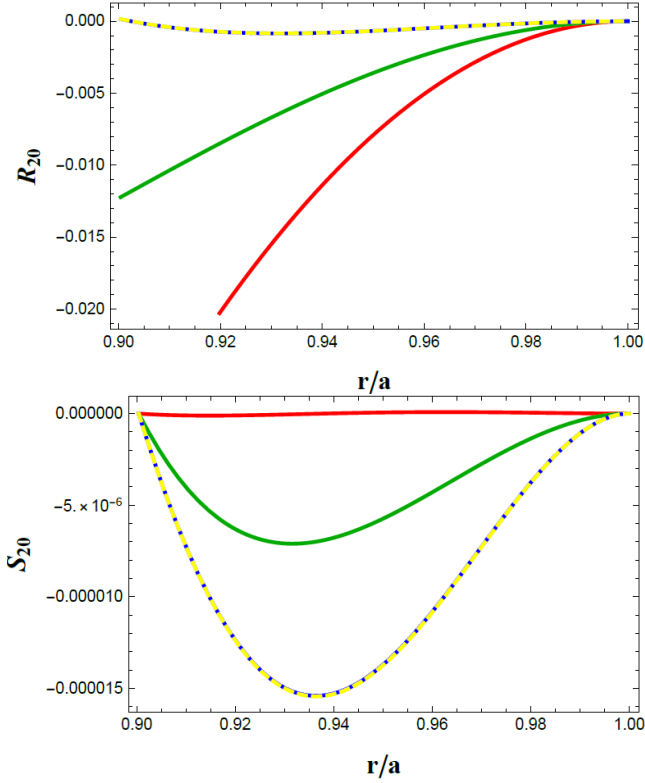


**Figure 11.** Normalized  $R_{20}(r)$  (top) and  $S_{20}(r)$  (bottom) stresses as function of the normalized radius. The plot refers to the crustal region, extending from  $r = r_c$  to  $r = a$ . We used different adiabatic indexes:  $\gamma = 2$  (red),  $\gamma = 2.1$  (green),  $\gamma = 200$  (blue) and  $\gamma = \infty$  (yellow dashed).

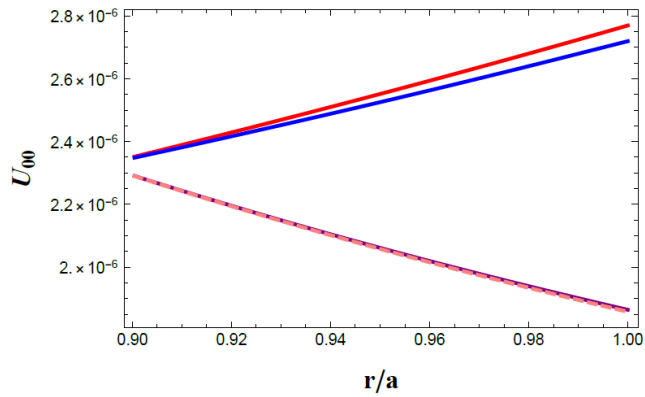


**Figure 12.** Normalized  $U_{00}(r)$  displacement as function of the normalized radius, in the region between  $r = r_c$  and  $r = a$ . As in the other figures, the curves refer to the results calculated by considering  $\gamma = 2$  (red),  $\gamma = 2.1$  (blue),  $\gamma = 200$  (purple) and  $\gamma = \infty$  (pink, dashed).

the usual  $M = 1.4 M_{\odot}$  star described by a polytrope  $n = 1$ , which stratification has been calculated both in the Newtonian and in General Relativity frameworks (i.e. by using the TOV equations). The difference between the two effective adiabatic indexes is shown in Fig 16.

In the Newtonian case the effective index is clearly given

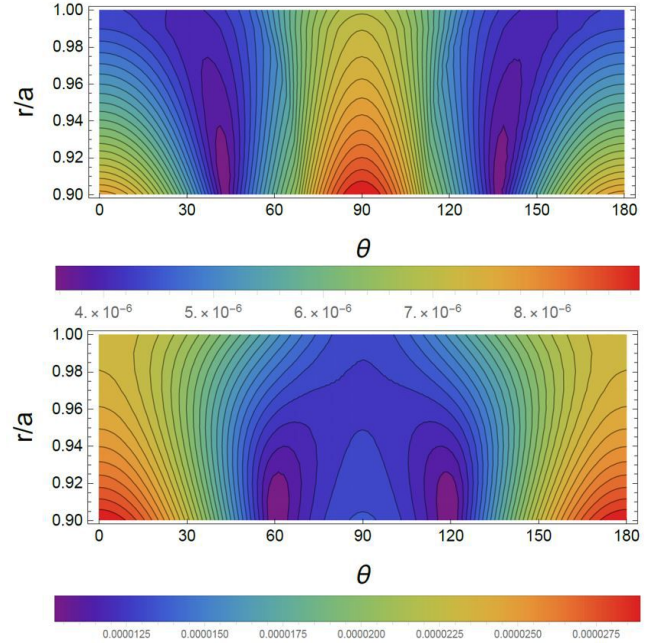


**Figure 13.** Color map of the normalized strain angle  $\tilde{\alpha}$  as a function of the colatitude  $\theta$  and of the normalized radius  $r/a$ . The region shown here refers to the crustal layer, from  $r = r_c$  to  $r = a$ . Our reference star of  $M = 1.4 M_{\odot}$  has been used, with different adiabatic indexes governing the perturbations:  $\gamma = 2.1$  (top) and  $\gamma = 200$  (bottom). Here  $\alpha$  for  $\gamma = \infty$  is not reported because it has the same shape and values of the case  $\gamma = 200$ .

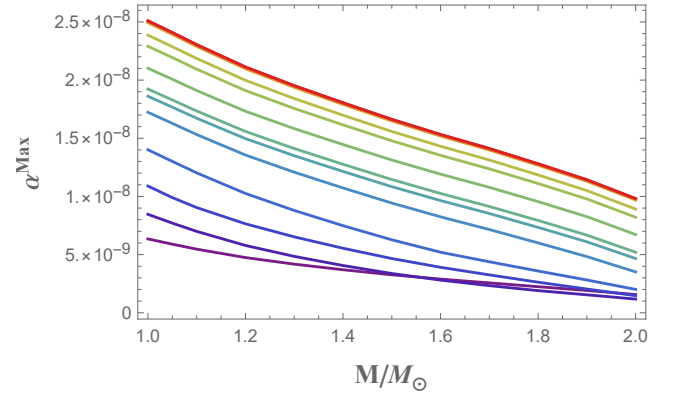


**Figure 14.** Maximum strain angle  $\alpha^{Max}$  as a function of the stellar mass, calculated for  $\Omega = 1$  rad/s and different adiabatic indexes ( $\gamma_f = 2, 2.05, 2.1, 2.2, 2.5, 2.8, 3, 4, 7, 12, 100$  and  $1000$ ) going monotonically from the lowest purple line ( $\gamma_f = 2$ ) to the red one on top ( $\gamma_f = 1000$ ). The curve for  $\gamma_f \geq 100$  is superimposed to the one for  $\gamma_f \geq 1000$ , indicating that the star's behaviour is essentially indistinguishable with respect to the incompressible limit. The purple line coincides with the curve in Fig 6.

by  $\gamma = 2$ , as it should be. However, when the TOV equations are employed in order to find the stellar stratification, there is a radial departure of the effective adiabatic index  $\gamma$  from this value, exceeding the 5% in the crust. This means that one cannot use a general relativistic density profile in a Newtonian model, since the star behaviour will always be



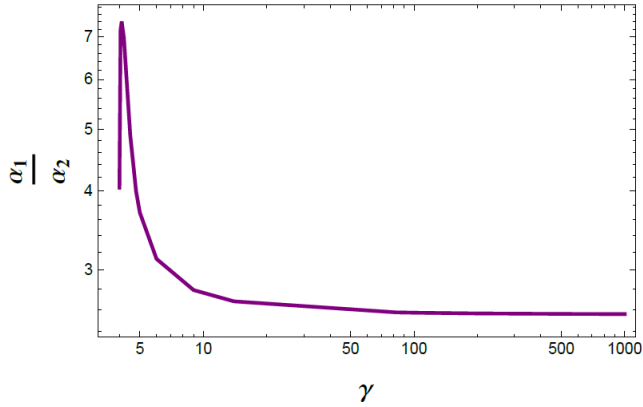


**Figure 15.** Ratio of maximum strain angle  $\alpha_{M=1M_\odot}^{Max}/\alpha_{M=2M_\odot}^{Max}$ , as function of the adiabatic index including both  $\ell = 0$  and  $\ell = 2$  harmonics contribution for  $\Omega = 1$  rad/s.

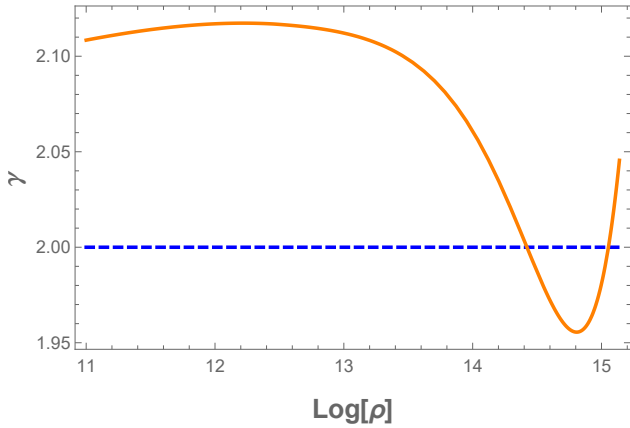


**Figure 16.** The effective adiabatic index calculated from the equilibrium configuration in General Relativity (orange) and in a Newtonian gravity (blue, dashed). Both the adiabatic indexes are shown for a  $M = 1.4M_\odot$  neutron star which EoS is given by the polytrope  $n = 1$ .

dominated by this out-of-control deviation of the effective adiabatic index.

## 6 APPLICATION TO PULSAR GLITCHES

Glitches are sudden jumps in the rotational frequency of a pulsar followed by a period of slow recovery that can last for several weeks or months. Despite many models have been used to study the glitch phenomenon, the trigger mechanism remains mysterious and the failure of the crust has been invoked since the first studies as a possible cause (as reviewed in [Haskell & Melatos 2015](#)).

We estimate the accumulated strain due to the spin-down of the pulsar in between two glitches in the Vela pulsar, which parameters  $\Omega$  and spin-down rate  $\dot{\Omega}$  are given in Tab 2. The same approach presented in ([Giliberti et al. 2018](#)) is used but employing the present, more refined, model for crustal deformations: the absolute difference in angular ve-

$\Omega$ (rad/s)	$\dot{\Omega}$ (rad/s <sup>2</sup> )	$\omega$ (rad/s)
70.338	$-9.846 \times 10^{-11}$	$80.44 \times 10^{-4}$

**Table 2.** The used rotational parameters and the average observed waiting time between two large glitches in the Vela pulsar.

locity between two Vela glitches is estimated as  $\omega \approx |\dot{\Omega}| \langle t_{gl} \rangle$ , where  $\langle t_{gl} \rangle \approx 3$  yr is the typical observed inter-glitch time.

The strain developed during the inter-glitch time due to the variation of  $\Omega$  can be estimated as

$$\alpha = \tilde{\alpha} (d(\Omega) - d(\Omega - \omega)) \approx \tilde{\alpha} \frac{2\Omega\omega a^2}{3v^2}, \quad (89)$$

where  $\tilde{\alpha}$  is the normalized strain angle and  $d(\Omega)$  is given in Eq (78). Using the parameters in Table 2, and assuming a typical mass of  $M = 1.4M_\odot$ , we get

$$\alpha_{Vela}^{Max} = 3.5 \times 10^{-4} \tilde{\alpha}, \quad (90)$$

which means that the strain accumulated due only to the spin-down between two glitches is of the order of

$$\alpha_{Vela}^{Max} = 2.1 \times 10^{-9}. \quad (91)$$

This is an extremely small value if compared to the assumed breaking strain in the range  $10^{-5} \div 10^{-1}$ : therefore, the crust's failure may be a viable trigger for glitches only in the eventuality that the crust is always stressed and very near to the breaking threshold. In other words, in order to trigger a sequence of glitches, the crust-quakes must release only an extremely small portion of the crustal stresses that have been accumulated up to that point.

## 7 CONCLUSION

In this paper we introduced a model to study the deformation of an self-gravitating and compressible neutron star under chosen loads: we focused on rotation, but we underline that this approach can be used also for tidal forces and non-conservative forces, like the stress induced by pinning of superfluid vortices in the crust. The analysis has been made in Newtonian gravity, while the realistic structure of the NS is introduced by considering a polytrope  $n = 1$  (i.e.  $\gamma_{eq} = 2$ ) which mass-radius relation has been calculated by using the EoS of [Douchin & Haensel \(2001\)](#). In this way our Newtonian model is consistent, in the sense that no spurious effects due to an artificial effective adiabatic index are introduced (as explained in section 5.3). This allowed us to study the effect of a possible departure of the adiabatic index from its equilibrium value ([Haensel et al. 2002](#)) during the build-up of stresses. In general, we find that the choice of the adiabatic index has great impact on the calculated displacement and stresses, as well as on the strain angle.

The study of the elastic response of a neutron star in the case of a non-equilibrium adiabatic index  $\gamma_f$  shows very interesting features. Despite the small difference in the value of adiabatic indexes in the cases  $\gamma_{eq} = 2$  and  $\gamma_f = 2.1$ , the dynamical responses of the model are clearly distinguishable, either for displacement, or stresses or strain angles. This fact is closely related to the smallness of the shear modulus with respect to the bulk modulus, as explained in section 5.2.

The sensitivity of strains and stresses to the actual value of the adiabatic index governing perturbations puts a severe

warning concerning a naive use of density profiles obtained via integration of the TOV equations in Newtonian models for stellar deformations: in fact, given the same EoS, the effective adiabatic index calculated by employing the relativistic stratification turns out to be quite different with respect to the value  $\gamma_{eq}$ , that is intrinsic to the EoS.

Therefore, in order to clearly separate the effect of inconsistent stratification from the one arising from the use of an frozen adiabatic index, a completely relativistic model is needed.

Finally, we explored the effects of the spin-down on a pulsar, confirming the result discussed in (Giliberti et al. 2018): the difference in angular velocity calculated between two different glitches gives rise to small strain angles, of the order of  $\alpha \sim (\Omega \delta \Omega / 1 \text{ rad}^2 \text{ s}^{-2}) \times 10^{-9}$  for a typical  $M = 1.4 M_\odot$  NS. These values are orders of magnitude smaller even with respect to the smallest breaking strain that is theoretically expected, of the order of  $10^{-5}$ .

Finally, we remark that the strain caused by the change in the rotation rate turns out to be a decreasing function of the stellar mass, as expected also in the incompressible cases previously studied by Franco et al. (2000) and Giliberti et al. (2018): with respect to low-mass neutron stars, the crust of a very compact and massive star is more difficult to deform by means of a change in the angular velocity. This suggests that, if starquakes are assumed as triggers of glitches, pulsars showing a dense sequence of timing irregularities should be lighter than pulsars showing sparse events.

## ACKNOWLEDGEMENTS

We thank the PHAROS COST Action (CA16214) and INFN for partial support. MA acknowledges support from the Polish National Science Centre grant SONATA BIS 2015/18/E/ST9/00577, P.I.: B. Haskell. MA and EG would like to thank Morgane Fortin, Leszek Zdunik and Pawel Haensel for valuable discussion.

## APPENDIX A: spherical harmonics

In this work spherical harmonics are defined as

$$Y_{\ell m}(\theta, \phi) = P_{\ell m}(\cos \theta) e^{im\phi}, \quad (\text{A1})$$

where  $P_{\ell m}$  are the Legendre polynomials, given by

$$P_{\ell m}(x) = \frac{(1-x^2)^{m/2}}{2^\ell \ell!} \frac{d^{\ell+m}}{dx^{\ell+m}} (x^2-1)^\ell \quad \text{if } m \geq 0$$

$$P_{\ell m}(x) = (-1)^m \frac{(\ell-m)!}{(\ell+m)!} P_{\ell m}(x) \quad \text{if } m < 0.$$

Therefore, spherical harmonics are eigenvalues of the angular part of the Laplacian, i.e.

$$\nabla^2 Y_{\ell m} = -\frac{\ell(\ell+1)}{r^2} Y_{\ell m}, \quad (\text{A2})$$

and are normalized as

$$\int_{\Omega} Y_{\ell m} Y_{\ell' m'}^* d\Omega = \frac{4\pi}{2\ell+1} \frac{(\ell+m)!}{(\ell-m)!} \delta_{\ell\ell'} \delta_{mm'}, \quad (\text{A3})$$

where  $d\Omega = \sin \theta d\theta d\phi$ . Consistently with the previous definitions, it is possible to expand the total incremental potential

$\Phi^\Delta$  as

$$\Phi^\Delta(r, \theta, \phi) = \sum_{\ell=0}^{\infty} \sum_{m=-\ell}^{\ell} \Phi_{\ell m}(r) Y_{\ell m}(\theta, \phi). \quad (\text{A4})$$

The expansion of vectorial quantities is more subtle: for example, the total displacement  $\mathbf{u}$  is decomposed in terms of the spheroidal  $\mathbf{u}_S$  and the toroidal  $\mathbf{u}_T$  displacements as

$$\mathbf{u} = \mathbf{u}_S + \mathbf{u}_T, \quad (\text{A5})$$

where

$$\mathbf{u}_S(r) = \sum_{\ell=0}^{\infty} \sum_{m=-\ell}^{\ell} [U_{\ell m}(r) \mathbf{R}_{\ell m}(\theta, \varphi) + V_{\ell m}(r) \mathbf{S}_{\ell m}(\theta, \varphi)]$$

$$\mathbf{u}_T(r) = \sum_{\ell=0}^{\infty} \sum_{m=-\ell}^{\ell} [W_{\ell m}(r) \mathbf{T}_{\ell m}(\theta, \varphi)].$$

In the above expansions, the symbols  $\mathbf{R}_{\ell m}, \mathbf{S}_{\ell m}, \mathbf{T}_{\ell m}$  are vectorial quantities defined by

$$\mathbf{R}_{\ell m} = Y_{\ell m} \mathbf{e}_r \quad (\text{A6})$$

$$\mathbf{S}_{\ell m} = r \nabla Y_{\ell m} = \partial_\theta Y_{\ell m} \mathbf{e}_\theta + \frac{1}{\sin \theta} \partial_\varphi Y_{\ell m} \mathbf{e}_\varphi \quad (\text{A7})$$

$$\mathbf{T}_{\ell m} = \nabla \times (r Y_{\ell m}) = \frac{1}{\sin \theta} \partial_\varphi Y_{\ell m} \mathbf{e}_\theta - \partial_\theta Y_{\ell m} \mathbf{e}_\varphi, \quad (\text{A8})$$

where  $\mathbf{e}_r, \mathbf{e}_\theta$  and  $\mathbf{e}_\varphi$  are the usual unit vectors of the spherical coordinate system.

The incremental stress acting on a spherical surface element with outward normal  $\mathbf{e}_r$  can be computed as

$$\boldsymbol{\sigma}^\delta \cdot \mathbf{e}_r = \sum_{\ell m} (R_{\ell m} \mathbf{R}_{\ell m} + S_{\ell m} \mathbf{S}_{\ell m} + T_{\ell m} \mathbf{T}_{\ell m}), \quad (\text{A9})$$

where

$$R_{\ell m} = \lambda \chi_{\ell m} + 2\mu \partial_r U_{\ell m}, \quad (\text{A10})$$

$$S_{\ell m} = \mu \left( \partial_r W_{\ell m} + \frac{U_{\ell m} - V_{\ell m}}{r} \right), \quad (\text{A11})$$

$$T_{\ell m} = \mu \left( \partial_r W_{\ell m} - \frac{W_{\ell m}}{r} \right). \quad (\text{A12})$$

We refer to  $R_{\ell m}$  and  $S_{\ell m}$  respectively as the *radial* and *tangential spheroidal* stresses. On the other hand,  $T_{\ell m}$  is called *toroidal stress*.

Finally, a generic non-conservative force  $\mathbf{h}$  can be expanded in terms of three real and independent sets of coefficients  $h_{\ell m}^R, h_{\ell m}^S$  and  $h_{\ell m}^T$  according to the formula

$$\mathbf{h} = \sum_{\ell=0}^{\infty} \sum_{m=-\ell}^{\ell} \left( h_{\ell m}^R \mathbf{R}_{\ell m} + h_{\ell m}^S \mathbf{S}_{\ell m} + h_{\ell m}^T \mathbf{T}_{\ell m} \right). \quad (\text{A13})$$

## APPENDIX B: the $\ell = 0$ harmonic

The matrix  $A_\ell(r)$ , for the harmonic  $\ell = 0$  is

$$A_0(r) = \begin{pmatrix} -\frac{2(\kappa - \frac{2}{3}\mu)}{r\beta} & \frac{1}{\beta} & 0 & 0 \\ \frac{4}{r} \left( \frac{3\kappa\mu}{r\beta} - \rho_0 g \right) & -\frac{4}{r} \frac{\mu}{\beta} & -\frac{\rho_0}{r} & \rho_0 \\ -4\pi G \rho_0 & 0 & -\frac{1}{r} & 1 \\ -\frac{4\pi G \rho_0}{r} & 0 & 0 & -\frac{1}{r} \end{pmatrix}, \quad (\text{B1})$$

where  $\beta = \kappa + \frac{4}{3}\mu$ . This expression can be obtained from the general form for the matrix  $A$  (see appendix C) by putting

$\ell = 0$  and neglecting the tangential displacement and stress. The equation that we have to solve is

$$\frac{d\mathbf{w}_{00}}{dr} = \mathbf{A}_0 \mathbf{w}_{00} + \mathbf{f}_{cen}, \quad (\text{B2})$$

where  $\mathbf{f}_{cen}$  is the centrifugal force vector

$$\mathbf{f}_{cen} = (0, f_{cen}, 0, 0) \quad (\text{B3})$$

and the spherical solution  $\mathbf{w}_{00}$  is the four-vector

$$\mathbf{w}(r) = (U(r), R(r), \Phi(r), Q(r)). \quad (\text{B4})$$

We underline that in this case the approach is different with respect to the one presented in Eq (12) for  $\ell \geq 2$ , since here the potential  $\Phi^\Delta$  coincides with the perturbed gravitational potential  $\phi^\Delta$ . It can be shown that the system (B2) can be simplified in a system for  $U$  and  $R$ . In this respect the general vector solution of Eq B2 can be written as

$$\mathbf{w}_{00}(r) = \begin{pmatrix} U^{reg}(r) & 0 \\ R^{reg}(r) & 0 \\ \Phi^{reg}(r) & 1 \\ \frac{\Phi^{reg}(r)}{r} & \frac{1}{r} \end{pmatrix} \begin{pmatrix} C_1 \\ C_2 \end{pmatrix} + \begin{pmatrix} U^f \\ R^f \\ \Phi^f \\ Q^f \end{pmatrix}. \quad (\text{B5})$$

The superscript *reg* indicates the regular solution of the associated homogeneous system; while *f* indicates a particular solution of (B2). Note that the constant  $C_2$  does not affect the radial displacement and the radial stress, that can be found by fixing the other constant  $C_1$ . This can be done by imposing the boundary conditions for the radial stress, namely

$$R_{00}(a) = 0. \quad (\text{B6})$$

To find the solutions of Eq (B5), we need some initial conditions. Here, for simplicity, we are looking only for the explicit solution for  $U_{00}$  and  $R_{00}$ . In the innermost part of the star, we can state that all the quantities  $\rho$ ,  $\kappa$  and  $\mu$  are constant, therefore

$$\rho = \rho_0, \quad \kappa = \kappa_0, \quad \mu = \mu_0 = 0. \quad (\text{B7})$$

With this assumption we find

$$\begin{aligned} U^{reg}(x) &= \frac{-x \cos x + \sin x}{x^2} \\ R^{reg}(x) &= \frac{4\sqrt{\pi/3}\sqrt{G\kappa_0\rho_0} \sin x}{x} \\ U^f(x) &= -\frac{3x\sqrt{3\kappa_0\Omega^2}}{32G^{3/2}\pi^{3/2}\rho_0^2} \\ R^f(x) &= -\frac{9\kappa_0\Omega^2}{8\pi G\rho_0}, \end{aligned}$$

where  $x = 4\sqrt{G\pi/(3\kappa_0)}r\rho_0$ .

## APPENDIX C: general form of the matrix $A$

In Eq (23), the spheroidal equations are written in a compact notation thanks to the use of the  $6 \times 6$  matrix  $A_\ell(r)$ , which general form is

$$A_\ell(r) = \begin{pmatrix} -\frac{2(\kappa-2/3\mu)}{r\beta} & \frac{\ell(\ell+1)(\kappa-2/3\mu)}{r\beta} & 0 & 0 & 0 & 0 \\ \frac{4}{r} \left( \frac{3\kappa\mu}{r\beta} - \rho_0 g \right) & \frac{\ell(\ell+1)}{r} \left( \rho_0 g - \frac{6\kappa\mu}{r\beta} \right) & 0 & 0 & 0 & 0 \\ \frac{1}{r} \left( \rho_0 g - \frac{6\mu\kappa}{r\beta} \right) & \frac{2\mu}{r^2} \left[ \ell(\ell+1) \left( 1 + \frac{(\kappa-2/3\mu)}{\beta} \right) - 1 \right] & 0 & 0 & 0 & 0 \\ -4\pi G\rho_0 & 0 & 0 & 0 & 0 & 0 \\ -\frac{4\pi G\rho_0(\ell+1)}{r} & \frac{4\pi G\rho_0\ell(\ell+1)}{r} & 0 & 0 & 0 & 0 \end{pmatrix}$$

$$\begin{pmatrix} 0 & 0 & 0 \\ \frac{1}{r} & 0 & 0 \\ \frac{\ell(\ell+1)}{r} & -\frac{\rho_0(\ell+1)}{r} & \rho_0 \\ -\frac{3}{r} & \frac{\rho_0}{r} & 0 \\ 0 & -\frac{\ell+1}{r} & 1 \\ 0 & 0 & \frac{\ell-1}{r} \end{pmatrix} \quad (\text{C1})$$

## REFERENCES

- Abbott B. P., et al., 2017, *ApJ*, **839**, 12
- Baiko D. A., Chugunov A. I., 2018, *MNRAS*, **480**, 5511
- Baym G., Pines D., 1971, *Annals of Physics*, **66**, 816
- Baym G., Pethick C., Pines D., Ruderman M., 1969, *Nature*, **224**, 872
- Blaes O., Blandford R., Goldreich P., Madau P., 1989, *ApJ*, **343**, 839
- Cambiotti G., Sabadini R., 2010, *Geophys. J. Int.*, **180**, 475
- Cambiotti G., Klemann V., sabadini R., 2013, *Geophys. J. Int.*, **193**, 1071
- Chamel N., Haensel P., 2008, *Living Reviews in Relativity*, **11**, 10
- Chanmugam G., 1977, *ApJ*, **217**, 799
- Cheng B., Epstein R., Guyer R., Young A., 1996, *Nature*, **382**, 518
- Christensen R., 2013, *The Theory of Materials Failure*. Oxford University Press
- Cutler C., Ushomirsky G., Link B., 2003, *ApJ*, **588**, 975
- Douchin F., Haensel P., 2001, *A&A*, **380**, 151
- Fattoyev F. J., Horowitz C. J., Lu H., 2018, preprint, ([arXiv:1804.04952](https://arxiv.org/abs/1804.04952))
- Franco L. M., Link B., Epstein R. I., 2000, *ApJ*, **543**, 987
- Gilbert F., Backus G., 1968, *Dynamics of Stratified Solids*, 394, 82
- Giliberti E., Cambiotti G., Antonelli M., Pizzochero P., 2018, arXiv e-prints, [p. arXiv:1809.08542](https://arxiv.org/abs/1809.08542)
- Gourgoulhon E., Haensel P., Gondek D., 1995, *A&A*, **294**, 747
- Gögüş E., Woods P. M., Kouveliotou C., van Paradijs J., Briggs M. S., Duncan R. C., Thompson C., 2000, *ApJ*, **532**, L121
- Haensel P., Levenfish K. P., Yakovlev D. G., 2002, *A&A*, **394**, 213
- Haensel P., Potekhin A. Y., Yakovlev D. G., eds, 2007, *Neutron Stars 1 : Equation of State and Structure Astrophysics and Space Science Library Vol. 326*
- Haskell B., Melatos A., 2015, *International Journal of Modern Physics D*, **24**, 1530008
- Haskell B., Jones D. I., Andersson N., 2006, *MNRAS*, **373**, 1423
- Horowitz C. J., Kadau K., 2009, *Phys. Rev. Lett.*, **102**, 191102
- Howitt G., Melatos A., Delaigle A., 2018, *ApJ*, **867**, 60
- Keer L., Jones D. I., 2015, *MNRAS*, **446**, 865
- Landau L., Lifshitz E., 1970, *Theory of Elasticity*. Pergamon Press
- Lander S. K., Gourgoulhios K. N., 2019, arXiv e-prints, [p. arXiv:1902.02121](https://arxiv.org/abs/1902.02121)
- Lander S. K., Andersson N., Antonopoulou D., Watts A. L., 2015, *MNRAS*, **449**, 2047
- Lasky P. D., 2015, *Publications of the Astronomical Society of Australia*, **32**, e034
- Link B., Franco L. M., Epstein R. I., 1998, *ApJ*, **508**, 838
- Love A., 1934, *A Treatise on the Mathematical Theory of Elasticity*. University Press, <https://books.google.pt/books?id=AD79MAAACAAJ>
- Melatos A., Peralta C., Wyithe J. S. B., 2008, *ApJ*, **672**, 1103
- Metzger B. D. W., Thorne K. S., 1966, *ApJ*, **145**, 514
- Pines D., 1974, *Nature*, **248**, 483
- Ruderman M., 1976, *ApJ*, **203**, 213
- Ruderman M., 1991a, *ApJ*, **366**, 261
- Ruderman M., 1991b, *ApJ*, **382**, 576

- Sabadini R., Vermeersen B., Cambiotti G., 2016, *Global Dynamics of the Earth: Applications of Viscoelastic Relaxation Theory to Solid-Earth and Planetary Geophysics*. Springer Netherlands, <https://books.google.pl/books?id=33xBDAAAQBAJ>
- Shapiro S., Teukolsky S., 1983, *Black holes, white dwarfs, and neutron stars: the physics of compact objects*. A Wiley-interscience publication, Wiley, <https://books.google.pl/books?id=KgF3fN3kaZAC>
- Thompson C., Duncan R. C., 1995, *MNRAS*, 275, 255
- Thorne K. S., Campolattaro A., 1967, *ApJ*, 149, 591
- Ushomirsky G., Cutler C., Bildsten L., 2000, *MNRAS*, 319, 902
- Woan G., Pitkin M. D., Haskell B., Jones D. I., Lasky P. D., 2018, preprint, ([arXiv:1806.02822](https://arxiv.org/abs/1806.02822))
- Zdunik J. L., Bejger M., Haensel P., 2008, *A&A*, 491, 489

This paper has been typeset from a  $\text{\TeX}/\text{\LaTeX}$  file prepared by the author.